DROPLETS, FILMS AND EDGES

DROPLETS, FILMS AND EDGES: STUDIES OF THE PHYSICAL CHARACTER OF DIBLOCK COPOLYMERS

By

ANDREW B. CROLL, B.Sc.

A Thesis
Submitted to the School of Graduate Studies
in Partial Fulfillment of the Requirements
for the Degree
Doctor of Philosophy

McMaster University

DOCTOR OF PHILOSOPHY (2008) McMaster University
(Physics) Hamilton, Ontario

TITLE: Droplets, films and edges: studies of the physical character of diblock copolymers

AUTHOR: Andrew B. Croll, B.Sc.(University of Waterloo)

SUPERVISOR: Dr. K. Dalnoki-Veress

NUMBER OF PAGES: viii, 44

Abstract

Block copolymers, long chain molecules of two distinct chemical species joined covalently to one another, have long been known to form organized structures on the nanoscopic level. For example, if the two chains are the same length a lamellar structure results. In this work we show how this internal structure causes distinct deviation from 'normal' fluid behavior. We begin with the observation of block copolymer droplets with atomic force microscopy. We note the droplets form nearly conical shapes in stark contrast to the usual spherical cap. These droplets are found to spread at an incredibly slow speed, and to have interesting instabilities in their wetting layer. We move on to studies of completely wet substrates (i.e. thin films) near the order-disorder transition of the material. Here we directly observe, with optical microscopy, a change in the fundamental spacing of the diblock's internal structure. This represents a superior method of measurement of the Flory-Huggins interaction parameter, which we verify in several ways. We also use the change in lamellar thickness to drive diffusion from one layer to another, and by similar measurements we can determine the kinetics of diffusion between the lamellar layers. In the last study we measure the lamellar edges on a gradient thickness sample with optical microscopy. In so doing we can directly observe surface induced ordering, and for the first time, can precisely resolve the near surface ordering dynamics.

Preface

This is a 'sandwich' thesis. As the published works are collaborations among several researchers some comments are necessary. I am the primary author of all works presented which represent experiments concieved of, conducted, and analyzed by myself. Often modern theoretical methods are of sufficient complexity that their implementation is beyond the humble experimenter. Therefore, we have relied upon the expertise of several top theorists in many of our papers (An-Chang Shi and Mark Matsen).

Acknowledgements

I would like to thank my parents for somehow helping me survive my adolescence. I am often surprised that they managed to do so. They are both intelligent people and it would not have been easy to become interested in a career in science if it were not so. They provide endless guidance and inspiration. My sisters, Lisa and Amy, are also both successful in their respective careers and give me a lot to look up to.

I could not have survived this far without the endless love and support of my wife Stacey. Her patience with me and with this foolish obstacle to a normal life is nothing short of completely irrational. Her putting her own professional life on hold for me is a true sacrifice, and it is greatly appreciated. I would also like to thank our first child, Elizabeth, for being an inspiration and the driving force behind my hard work. Children need successful parents, and I am trying my best to be that for her (and any subsequent children that we might be lucky enough to have). These two are everything to me.

Kari has also provided a great environment for one to work in. There is never any shortage of enthusiasm or funding, and he has been very good to allow me such complete creative freedom. He has taken me to meetings, introduced me to other esteemed scientists, and tried to provide a good start to my career. I do appreciate all he has done.

Finally I would like to thank all the lab-rats of the Dalnoki-Veress group who are an endless source of good times. Adam Raegen, who started with me, has always been there to discuss my work and offer his two cents. I have also appreciated, and learned from his work which he has always shared with me. Matt Farrar the summer student that I most closely worked with, and whom I must apologize to for not including the projects that he helped me with in this thesis. Rob Welch, my second summer student, who also did great work that I have not had time to finish yet(sorry!). Mike Massa who was here to show me the ropes, AFM, and the diblock drops. Marie-Joseé Colbert and Jessica Carvalho, whom I did not get to work with, but have enjoyed conversation and support from both of them. Josh McGraw and Marc-Antoni Goulet, the old new guys, who have now both got master's under their belt and technically

(although hopefully briefly) out rank me. And thanks to all the Faculty, staff and students at McMaster with whom I have been privileged to work with.

Finally, thanks to Trouble the Cat whose incessant disruption of my towers of papers has undoubtedly uncovered important ideas in this research.

Contents

List of Figures

Chapter 1

Introduction

Block copolymers, those "clever animals that can find their way to an interface" [1], are one of the most fascinating molecules of modern synthetic materials. They have properties that are similar to those of lipids, of liquid crystals and, of course, of polymers, which places them firmly at the crossroads of modern soft condensed matter. They spontaneously form structure on a nanoscopic scale, making them of clear relevance in modern lithographic technology [2]. They make polymer alloys (blends) stronger [3]. They are complex. They are beautiful. They are the backbone of this thesis.

To appreciate the physics of block copolymers, one must first be introduced to some of the physics behind ordinary long chain *polymer* molecules. This is because a block copolymer is made of several different long chains that are joined together by a chemical bond. One must also be acquainted with the details of phase separation, as many of the most interesting properties of block copolymers arise because the different blocks are unable to mix. Only after familiarization of these two topics can one delve into the introductory physical details of diblock copolymers (the simplest form of a block copolymer, in which two different polymers are joined at one end). Study of these physical details, such as the micro-phase separated state in which these materials spontaneously form nanoscopically ordered structures, will be continued throughout this thesis. After an introduction to these background concepts, the first experimental work of this thesis will be presented. These experiments will begin by

looking at static and dynamic aspects of small droplets of fluid on a silicon substrate. These studies reveal that ordered symmetric diblock copolymers form a near-conical structure, in stark contrast to the familiar spherical shape adopted by ordinary fluids. The dynamics of spreading is found to be dramatically slowed, and to depend primarily on molecular friction rather than a true newtonian viscosity. Finally, we find that molecular details of the thin wetting fluid layer at the base of a spreading droplet leads to a unique fingering instability which is analogous to the process by which snowflakes form such unique shapes [4].

In chapter 3 we discuss experiments on thin films of diblock copolymer that completely cover a substrate. In these experiments we observe the spacing of the internal layers of the fluid precisely, and by changing the sample temperature, build up directly a map of layer spacing as a function of temperature.. These results lead us to make several conclusions about the scaling of this thickness near the order to disorder transition, primarily of note is that this region is not well approximated by a single power law function. We also observe the dynamics of the relaxation from one equilibrium spacing to another as temperature is changed.

We next study how the material forms ordered structures near the substrate while the bulk remains in the disordered state [5–7]. Our experiment allows us to make high resolution measurements of the location of the ODT, which we note to be significantly above the simple mean field prediction. This non-mean field ODT is in line with current understanding of fluctuation effects [6,8]. The same experimental system also allows for simple real-space observation of the ordering and disordering dynamics of these surface layers. Finally, we repeat these last two experiments using an alternative variable and a second polymer. The agreement of this second set of data lends great confidence to our new understanding.

1.1 Polymers

Polymers are molecules created through the repetition of a large number of units known as monomers. These molecules have an exceptional aspect ratio, often being of order 10^6. As one might imagine, the result of this extreme aspect ratio is an incredibly

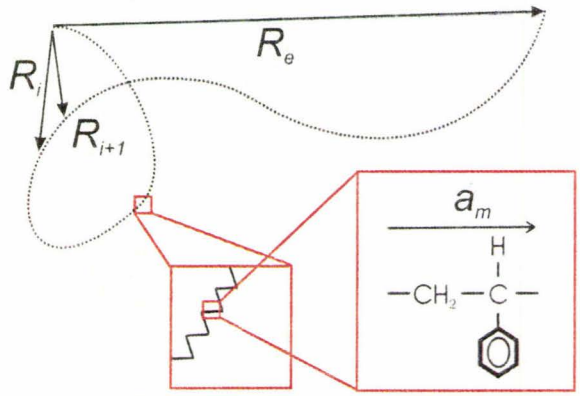

Figure 1.1: The geometry of a polymer chain in the coarse-grained model used throughout this thesis. Boxes show progressively magnified regions of chain, the limit of which is the true chemical structure.

flexible molecule. Indeed, as will be shown shortly, this flexibility dominates most of the properties that make polymeric materials so desirable (elasticity, toughness, processibility, ...). The flexibility is determined by the geometry of the molecules. It is therefore easy to see why a coarse grained view of these materials is so desirable - the properties do not strongly depend on the type of monomer used.

In the spirit of generalization we will persue the standard treatment followed by many authors [9, 10] and consider an object of N_m monomers each of length $|\vec{c}_i|$. The vector $\vec{c}_l$ points along the backbone of the lth monomer in the chain (see Fig. 1.1). We also note N_m is a very large number. Any two adjacent monomers (say at positions R_i and R_{i+1}) will be related to each other by some well defined bond angle, θ. This angle, and the size $|\vec{c}_i|$, are strongly related to the type of monomer used. We therefore wish to find a lengthscale at which we lose this level of detail. To set this new lengthscale we consider a vector $\vec{a}_i$ which we define as the sum of several monomer vectors ($\vec{a}_i = \sum_{l=i}^{i+n} \vec{c}_l$). The key is that $\vec{a}_i$ is large enough that $\langle \vec{a}_i \cdot \vec{a}_{i+1} \rangle \approx 0$, that is, the vectors $\vec{a}_i$ and $\vec{a}_{i+1}$ are completely uncorrelated. The result is that the trajectory of the chain of uncorrelated links follows a random walk of step length $a = |\vec{a}|$ [9, 10].

Before discussing the random-walk or 'ideal' polymer chain, there remains one ambiguity in the model that must be addressed - we have no definition for n, the number of monomers in a segment of length $|\vec{a}_i|$. The lower limit of n is set by

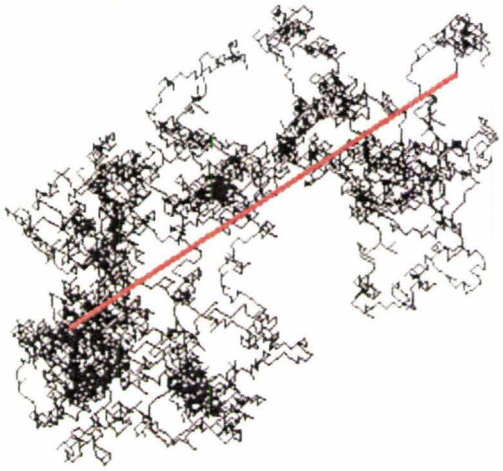

Figure 1.2: A 1000 step random walk on a cubic lattice. The solid red line connects the two ends of the chain (i.e. it is $\vec{R}_e$).

the requirement of zero correlation between segments, but the upper limit remains unbound. Kuhn was the first to suggest using the requirement of equal trajectory of the ideal and real chain to set this limit [9]. Specifically, we require that $|\vec{c}|N_m = |\vec{a}|N$. With this we have a complete definition, the Kuhn length, $|\vec{a}|$, is the length which is small enough that there is no correlation between two adjacent units, but not large enough to change the total contour length.

A useful way to visualize this generalization is to use a lattice model to simulate a polymer chain [11, 12]. In a lattice model, space is discritized into points that lie on a lattice (a cubic lattice is shown in figure 1.2). A polymer is then represented by connecting lattice points together to form a chain. Such simulations give direct access to all of the details that have just been discussed, for example, $\vec{R}_e$ is shown in Fig. 1.2. This simple type of model is useful in construction of heuristic, analytic models of polymer behavior that capture the essential physics of a situation. This type of model will be relied upon heavily in the following discussion.

As we have mentioned this ideal polymer chain follows a random walk contour in

space. This is convenient as it allows the use of the many textbooks devoted to the Gaussian statistics of random walks [13,14]. Therefore we simply note several features of the Gaussian chain result, starting with a definition of the distribution function, $p(\vec{R}_e)$, where $\vec{R}_e$ is the average end to end vector [10]. This function can be thought of as a map of probabilities of having a random walk with and end to end vector given by $\vec{R}_e$. It is given by,

$$p(R_e) = k^{-3/2} exp\Big(- \frac{3|\vec{R}_e|^2}{2k^2} \Big); \tag{1.1}$$

where k is the root mean squared average value of $\vec{R}_e$. The details of this new length, k, can be found directly from our 'ideal' chain model.

We begin by defining the end to end vector as,

$$\vec{R}_e = \sum_{i=0}^{N} \vec{a}_i, \tag{1.2}$$

from which we can then calculate k as follows,

$$k = \sqrt{\langle \vec{R}_e^{\,2} \rangle} = \sqrt{\sum_{i,j=0}^{N} \langle \vec{a}_i \cdot \vec{a}_j \rangle}. \tag{1.3}$$

However, $\vec{a}_i$ and $\vec{a}_j$ are uncorrelated, so this can be simplified to

$$k = a\sqrt{N}. \tag{1.4}$$

This simple scaling rule is one of the most important results of polymer physics and is commonly recast as the related quantity, $R_g = a\sqrt{N/6}$, the radius of gyration. This statement might be unexpected; one might have assumed that the total length of a polymer chain would appear in any relevant argument pertaining to material properties. As we shall show below, the average end-to-end size is indeed the most fundamental length in polymeric materials because of the dominance of entropy in these molecules.

To see how Eq. 1.4 is so intimately linked to material performance, let us now consider the free energy of a polymer chain in a melt with the particular end-to-end

distance R. The Gibbs free energy is given as

$$F = U - TS, \tag{1.5}$$

where U is an internal energy, T is temperature and S is the entropy. The internal energy of a chain in a melt will simply be a constant as polymers in the melt typically do not bond with other chains or break into pieces. This means the major contribution to the free energy is from entropy, which is easily calculated,

$$S \sim ln[p(R)] = S_0 - \frac{3R^2}{12R_g^2}; \tag{1.6}$$

where S_0 is a constant. Eq. 1.6 taken together with Eq. 1.5 show the dramatic effect of conformation on the fundamental properties of a polymer melt. If chains are stretched, there is a high energetic cost proportional to the square of the new end-to-end distance. This cost scales as the inverse of the radius of gyration squared, illustrating the importance of R_g to the physical properties of a polymer melt.

The resulting free energy is identical to the case of a simple spring ($F \sim kx^2$), which makes it clear why polymeric materials have a high elasticity. We further note that the polymeric 'spring constant' also depends directly on temperature. This important detail will be useful in understanding experiments that manipulate the chain conformations - high temperatures increase the cost of deviating from the average shape.

In summary, polymer chains can be successfully described as random walks [9, 10] This allows the identification of a statistical lenghtscale, R_g, which characterizes the average size of a polymer chain in the melt. The lengthscale, R_g, is important in quantifying many physical properties of a polymer melt, as for example, in the calculation of the free energy of a chain. Because of the dominance of entropy in these systems we expect temperature to greatly influence the physical properties of polymer melts (as $F \sim -TS$).

1.2 Polymer Blends

A polymer blend is created when one mixes two different polymers (say A and B). Blends can lead to useful combinations of material properties (for example, High Impact Polystyrene a common class of industrially important plastics, combine the hardness of styrene with the elasticity of butadiene) which makes them of significant interest to industry [15]. From a more fundamental point of view, the blend can lead to significant interphase formation [11], pattern formation [16], and interesting dynamics [17]. The characterization of these phenomena allows a deeper understanding of the interaction between polymers, and will form a starting point for our studies of diblock copolymers.

We begin by considering the free energy of mixing, which will ultimately allow us to characterize the blend [9, 11, 12]. This is the difference between the Gibbs free energy of a volume of A molecules, V_A, and a volume of B molecules, V_B, in an unmixed state and that of a volume, V, of a mixture of A and B molecules. We use this difference in free energy, rather than the full free energy, as many terms will not change between these two states and will simply serve to obfuscate the important parameters. We wish to create a microscopic model that allows us insight into the change in free energy,

$$\begin{aligned} \Delta F &= F_{AB} - F_A - F_B \\ &= -TS_{trans} + F_{int}; \end{aligned} \tag{1.7}$$

where S_{trans} is due to the gain in translational freedom of the molecules and F_{int} is due to the interaction of the different molecular species. For simplicity, let $V = V_A + V_B$, and the concentration of A molecules be represented as $\phi_A = V_A/V$. The entropy is given by,

$$S_{trans} = k_B\left[\frac{\phi_A}{N_A} ln(\phi_A) + \frac{(\phi_B)}{N_B} ln(\phi_B)\right]; \tag{1.8}$$

where N_A (N_B) is the number of monomers in the A (B) chain, and the first and second term are due to chain A and chain B respectively. This formulation arises from the conventional Gibbs formula, $S = k_B\ p\ ln(p)$; where k_B is the Boltzmann

constant and the probability is given by p. Here, the probability of finding a chain is simply the volume occupied by the chain in the total volume of the system. We must also account for the fact that N_A monomers belong to any A chain.

The calculation is most easily performed in a lattice model. We simply count occupied sites to arrive at a measure of entropy. The lattice also provides a convenient way calculate the interaction energy F_{int}. If we consider only nearest neighbour interactions we have three possible energies which we must sum up, ϵ_{AA}, the energy between two A monomers, ϵ_{BB}, the energy between two B monomers, and ϵ_{AB}, the energy between an A and B monomer. The lattice is filled with ϕ_A monomers which we assume interact with an average background. The average is a *mean field* assumption - a chain reacts to a 'field' created by all other molecules. The average field will be due to Z neighbours, which have a probability of being A (or B) given by ϕ (or $1-\phi$). By subtracting the energy of a chain in its unmixed state (i.e. $z\phi_A\epsilon_{AA} + z\phi_B\epsilon_{BB}$) we arrive at,

$$F_{int} = z[\phi_A(\phi_A - 1)\epsilon_{AA} + \phi_B(\phi_B - 1)\epsilon_{BB} + 2\phi_B\phi_A\epsilon_{AB}]. \tag{1.9}$$

We define $\chi \equiv z(-\epsilon_{AA} - \epsilon_{BB} + 2\epsilon_{AB})/k_BT$ where χ is known as the Flory-Huggins interaction parameter. If we assume incompressibility of the melt, $\phi_A + \phi_B = 1$, then

$$F_{int} = \phi(1-\phi)\chi kT. \tag{1.10}$$

We may now write the total Flory-Huggins free energy of mixing [18–20] as,

$$\Delta F/k_BT = -\left[\frac{\phi}{N_A}ln(\phi) + \frac{(1-\phi)}{N_B}ln(1-\phi)\right] + \phi(1-\phi)\chi \tag{1.11}$$

from which several observations are warranted. Firstly, although we have 'defined' a parameter χ as a purely energetic parameter it is unlikely that this is the case [9,21]. In general the interaction parameter is written as $\chi = \chi_H/T + \chi_S$, where the first term is the enthalpic term just discussed. The second term is a 'catch all' termed the entropic contribution due to the thermodynamical relation $S = -\delta F/\delta T$. There are many physical possibilities for this entropy (and indeed, extra contributions to the enthalpy), but the most relevant to our discussion is the unphysical nature of a simple

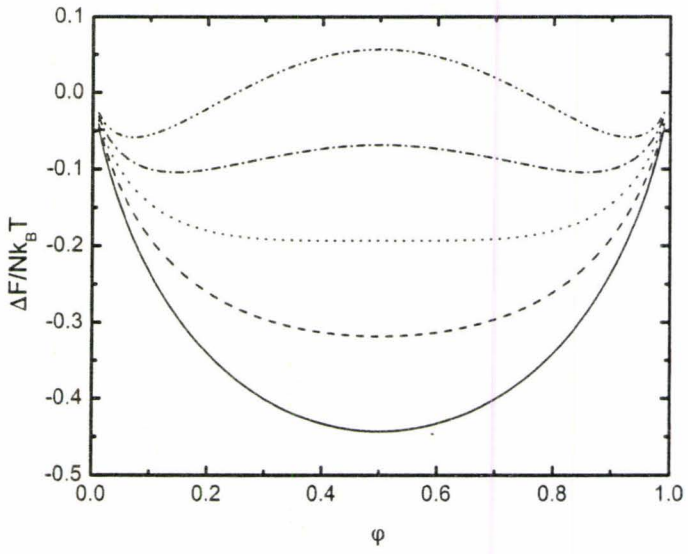

Figure 1.3: A plot of free energy per monomer as a function of weight fraction for several different values of χN. From the top down $\chi N = 3, 2.5, 2, 1.5, 1$.

lattice used in deriving χ (for an alternative see [22]).

With Eq. 1.11 we may now begin to describe the behavior of a polymer blend. For simplicity, let us consider a symmetric blend where $\phi_A = \phi_B$ and the polymer lengths are also equal $N = N_A = N_B$. We can then plot the resulting free energy of mixing per polymer for several different χN (see Fig. 1.3). The rescaling of χ for a simple molecular blend to χN for a polymeric mixture is introduced in order to illuminate the relevance of this combination of χ and N as the new enthalpic scale. Clearly a polymer of N units will have N interactions with the mixture, wheras a molecule of a simple fluid would only have one. The free energy changes from a function with a single minimum ($\chi N < 2$), to a function with two minima ($\chi N > 2$). The significance of this transition is clear when considering a particular mixture, for example a homogeneous mixture at ϕ' and $\delta F'$ and a separated mixture at some ϕ_a and ϕ_b. If χN is low the free energy is concave up and any separated state will have a free energy larger than $\delta F'$, as the new free energy is a weighted average of the two new free energies. This is most directly seen as the intersection of a vertical line through ϕ' and a line connecting $F(\phi_a)$ and $F(\phi_b)$ (see Fig. 1.4) [9].

Increasing the value of χN, we eventually find a case in which the free energy of

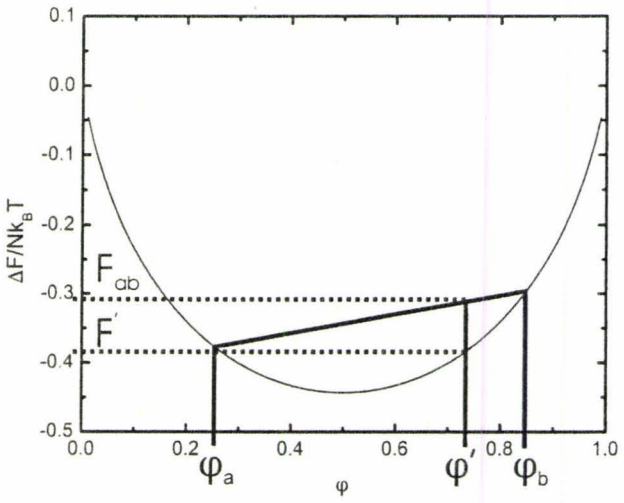

Figure 1.4: An illustration of the free energy per monomer as a function of weight fraction for $\chi N = 1$. A particular mixture initially of concentration ϕ' and energy F' will have a higher energy, F_{ab}, if it phase separates to concentrations ϕ_a and ϕ_b.

the phase separated mixture is lower than the homogeneous state. This means the mixture will have regions rich in A molecules, ϕ_a, in equilibrium with regions rich in B molecules, ϕ_b. The mixture has *phase separated.* The behavior crosses over as the concavity of the curve changes from positive to negative, allowing a rigorous definition of the boundary between mixed and demixed solution,

$$\frac{\partial F}{\partial \phi} = 0. \tag{1.12}$$

Eqn. 1.12 defines a new curve is known as the *binodal* line, and is most compactly written as

$$\chi N = \frac{1}{1-2\phi} ln\Big(\frac{1-\phi}{\phi}\Big); \tag{1.13}$$

where we see more clearly why χN is used in combination to describe the phase. χN is adequate to entirely describe the phase of a mixture - for χN above Eq. 1.13 there is phase separation, below it there is a homogeneous mixture.

There remains an important subtlety. There are conditions under which a mixture can be locally stable, even if the ultimate equilibrium state lowers the free energy.

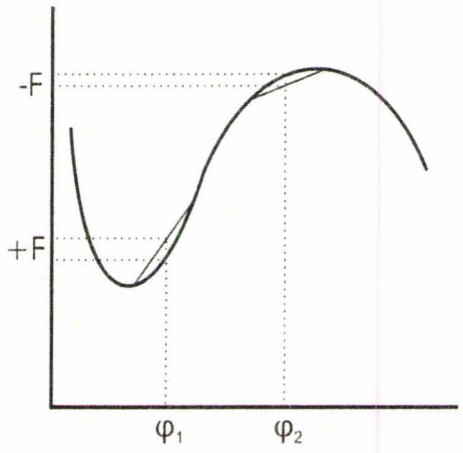

Figure 1.5: A schematic illustrating both metastable and unstable mixtures. A mixture at ϕ_2 is spontaneously unstable, any fluctuation is seen to lower the total free energy (by an amount -F). A mixture at ϕ_1 will have an increase in free energy (+F) with a small fluctuation even though a large fluctuation will lower the free energy.

This difference is illustrated in figure 1.5 where we see two mixtures ϕ_1 and ϕ_2. If we consider a small fluctuation of phase around these two points we find that the free energy is lowered for ϕ_2 and raised for ϕ_1. Hence, ϕ_2 will be unstable to any fluctuation, but ϕ_1 is not. The mixture at ϕ_1 must have a fluctuation of a large size before its energy is lowered - it must overcome a *barrier* before phase separating. These two cases are clearly delineated by a change in curvature of F, i.e.

$$\frac{\partial^2 F}{\partial \phi^2} = 0, \tag{1.14}$$

which leads to

$$\chi N = \frac{1}{2}\left(\frac{1}{\phi} + \frac{1}{1-\phi}\right). \tag{1.15}$$

This second curve is known as the *spinodal* line.

With these two curves we can now construct a comprehensive *phase diagram* (see Fig. 1.6). This diagram shows that a mixture will be spontaneously unstable for high χN and ϕ not to near 1 or 0. We also note that the metastable region fills a thin strip between the spinodal and binodal curves except for a point at $\phi = 1/2$ where the two curves meet. This point has thermodynamic significance which is revealed by

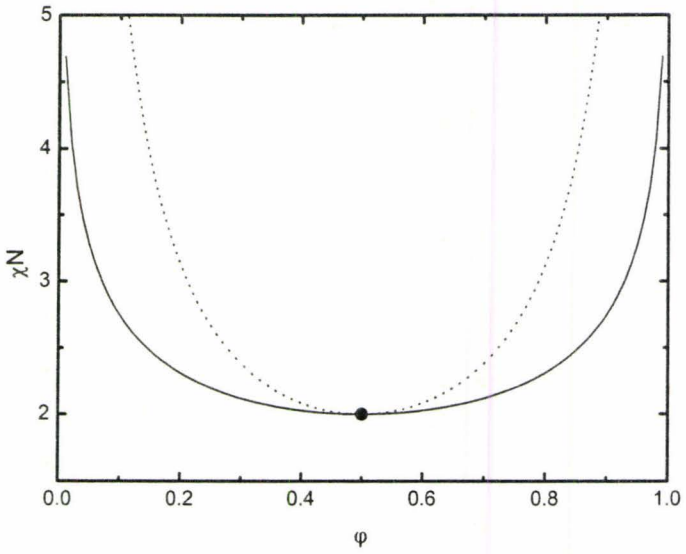

Figure 1.6: The phase diagram of a binary mixture. The solid line is the binodal and the dashed line shows the spinodal. Both lines converge on a critical point.

considering the order of the phase transition along the binodal. To do so most simply, we Taylor expand $F(\phi)$ around the binodal point ϕ_b. For points other than $\phi_b = 1/2$ we note that the term proportional to $(\phi - \phi_b)^3$ exists and therefore the transition is first order. However, for the special case of $\phi = 1/2$ we see that the third order derivative is identically zero, and the third order term of the expansion disappears. This means that there is a second order phase transition, and $\phi = 1/2$ is called a *critical point.*

Despite the mixture ultimately ending in a phase separated state, the metastable and unstable regions significantly differ in the kinetics of phase separation which leads to dramatic morphological differences [9,11,12,14]. In the metastable region a sample must overcome a barrier before separating into an A-rich and B-rich region. As a result the kinetics will follow the Arrhenius form,

$$\nu \sim e^{-\frac{\delta\epsilon}{k_b T}}; \tag{1.16}$$

where ν is a nucleation rate, and $\delta\epsilon$ is the size of the energy barrier.

The form of the energy barrier can be estimated by considering a small spherical

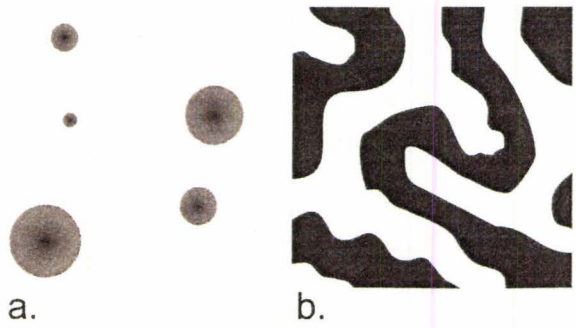

Figure 1.7: Schematic of the phase separation morphology of a. nucleation and growth regime and b. spinodal regime

domain of phase separated mixture. This domain will lower the system's free energy by δf times its volume ($\sim r^3$), where δf is simply the difference of free energy between the phase separated and phase mixed states. The domain also has an unfavourable interfacial tension γ which leads to

$$\delta\epsilon \sim -\delta f r^3 + \gamma r^2, \tag{1.17}$$

the standard form of classical nucleation theory [12]. Eqn. 1.17 has a single maximum, which is the barrier energy needed, i.e. $\delta\epsilon \sim \pi\gamma/\delta f$. The stochastic nature of the Arrhenius process means that the metastable region is dominated by random processes and as a result will have a morphology of many droplets of phase separated material of different sizes in uncorrelated locations (Fig. 1.7 a.).

Experiments on symmetric mixtures in the spontaneously unstable region (above the spinodal line) region typically show an interesting pattern of interconnected regions of A or B rich regions of similar size (see Fig. 1.7 b.), which is very different from the nucleation and growth morphology. In the spinodal region the kinetics are significantly faster as any thermal fluctuation instantly lowers the system's free energy. Because of the significance of the fluctuations there is no well defined surface between A and B rich regions, which means analysis similar to that of the nucleation regime (where the energies of surfaces and volumes are calculated) is destined to fail.

In order to evaluate the striking pattern formation in the spontaneously unstable

region of the phase diagram, we follow the Cahn-Hillard derivation [23] and begin with a free energy functional of the following form,

$$f(\phi) = \int \partial x \Big[f_0(\phi) + \kappa \Big(\frac{\partial \phi}{\partial x} \Big) \Big], \tag{1.18}$$

where κ is the gradient energy composition, $f_0(\phi)$ is the free energy in the phase mixed state, and we have integrated over the system in one dimension for simplicity [23]. This phenomenological form for the free energy takes the weak interface between A and B domains into account by considering the gradient explicitly [12]. The chemical potential is thus given by,

$$\begin{aligned} \mu &= \frac{\partial f(\phi)}{\partial \phi} \\ &= \frac{\partial f_0}{\partial \phi} + 2\kappa \frac{\partial^2 \phi}{\partial x^2}. \end{aligned} \tag{1.19}$$

As the chemical potential gradient drives the formation of the domains, this is all that is necessary to understand the pattern that forms. Molecules are driven by a chemical potential, and diffuse accordingly.

The pattern forms because a particular fluctuation diffuses more readily than others. This can be understood qualitatively as a contrast between the long distances material must diffuse in a long wavelength instability, and the high energetic cost of the many interphases formed in a short wavelength instability. Clearly some intermediate wavelength is the most relevant to the pattern. To be more rigorous, let us consider a *linearized* diffusion equation,

$$\begin{aligned} \frac{\partial \phi}{\partial t} &= m \frac{\partial^2}{\partial x^2} \mu \\ &= m f_0'' \frac{\partial^2 \phi}{\partial x^2} + 2m\kappa \frac{\partial^4 \phi}{\partial x^4}; \end{aligned} \tag{1.20}$$

where t is time, m is the mobility, and the linearization pertains to m and κ which are assumed to be only weakly dependent on ϕ. This is known as the Cahn-Hillard

equation [23]. Its solution is,

$$\phi = \phi_0 + e^{iqx} e^{-(mf_0''q^2 - 2m\kappa q^4)t}. \tag{1.21}$$

The fastest growing wave is simply the extrema of the argument of the second exponential ($q = \sqrt{f_0''/\kappa}$), and it is this lengthscale that best describes the morphology observed.

The phenomenological description of the statics and dynamics of binary mixtures, while not exact, is nonetheless a very good description of the physical process. This analysis will prove invaluable as a starting point for much of the discussion in the rest of this thesis. We will, in fact, find several instances where identical reasoning will allow us to understand the behavior of diblock copolymers.

1.3 Diblock Copolymers

Diblock copolymers, the main object of study of this thesis, are created by joining two chemically different polymers together at one end (see Fig. 1.8). This results in a peculiar type of polymer blend that has many fascinating properties; the most remarkable of which is the self-assembly of intricate nanoscopic patterns in a diblock copolymer melt [24]. These structures are of clear technological importance, given the desired small size of semiconductor hetrostructures [2]. Beyond the potential for technological use, diblocks form ideal model systems for the study of pattern formation, and offer a more easily controled analogy to the surfactant systems which are so abundant in Nature [25, 26].

As in an ordinary blend, the two blocks have an enthalpic interaction which can be characterized by the Flory-Huggins interaction parameter, χ [12, 24, 27]. Diblocks will also phase separate into A-rich and B-rich domains if χ exceeds some critical value. However, in the case of diblocks, we find that the process is frustrated by the connectivity of the two chains and stalls at some small lengthscale, L, that is dependent on the size of the chains. The diblock copolymer melt *microphase* separates into one of many possible nanostructures [24, 27].

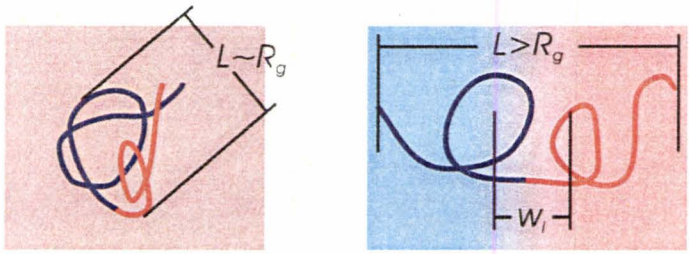

Figure 1.8: A diblock copolymer in its disordered and ordered state. The width of the $A-B$ interface is given as w_i and L characterises the most relevant lengthscale.

The simplest three nanostructures (spheres, cylinders and lamella) are illustrated in fig. 1.9, which shows a schematic phase diagram [28]. The particular structure is determined by the ratio of lengths of the two blocks, $f = N_A/(N_A + N_B)$. If the A block is very small, its enthalpic contribution will be ignored, and the melt will behave as a homopolymer melt of B molecules. As A becomes longer the interfacial energy grows and microphase separation into a body-centered lattice of spherical domains of A in a matrix of B takes place. The curved interface is mainly due to the geometry, since there is less A than B. As the A block becomes longer, the cost of deforming the molecules becomes greater and the spherical structure gives way to a hexagonally packed lattice of cylindrical domains. When A becomes comparable to B in length, there is a similar amount of both blocks and the interface becomes flat. The result is a lamellar structure for symmetric molecules. The phase is symmetric around $f = 0.5$, the location of A and B in the structures simply swap when A becomes longer than B.

The structures (and their spacing) can be accurately predicted if the correct free energy is known [24,25,29–31]. There are in fact several viable theories of the structure of diblock copolymers, each applicable in different ways. The simplest theoretical regime applies to the strongly segregated part of the phase diagram ($\chi N >> 10$). Here we may assume an extremely thin interface w_i between the different blocks (see Fig. 1.8b.) [12, 30, 31]. This assumption allows us to replace the interface by an energy cost per area, γ_{AB}, which competes with a stretching energy due to the loss of conformations by forcing the blocks to reside on their respective sides of the interface.

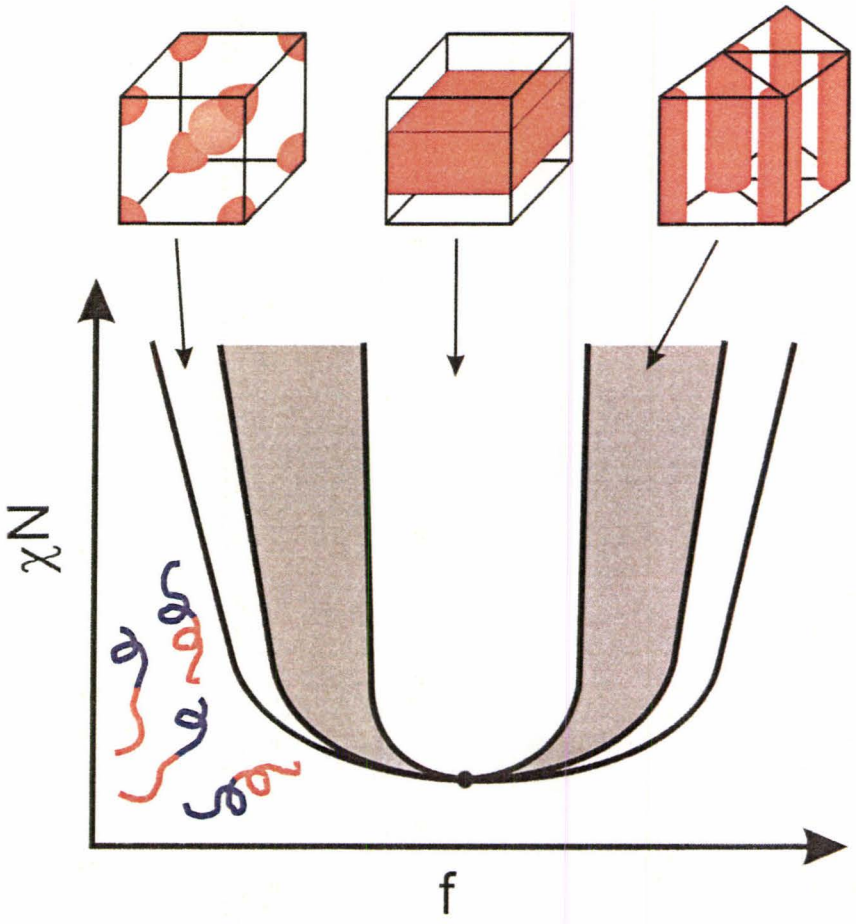

Figure 1.9: A schematic diblock copolymer phase diagram illustrating the four classical phases. Below the curve is the disordered phase. Immediately above this is the spherical phase, and then the hexagonally packed cylindrical phase. The largest central region represents the lamellar phase.

This stretching entropy is given by Eq. 1.6, resulting in the free energy,

$$F/k_BT = \frac{3L^2}{8Na^2} - \frac{\gamma_{AB}Na^3}{L}; \tag{1.22}$$

where $N = N_A + N_B$, and $a = (a_A + a_B)/2$ for simplicity. The latter definition is valid in the case that the two monomers share the same segment length, but forms a reasonable estimate otherwise.

In order to calculate the interfacial tension, the width of the interface must be determined. While there are more sophisticated methods of making this estimate [30, 32], we shall follow the simplest estimate in order to illustrate the relevant ideas [12]. We start by noting the interfacial width will be set by the length of some segment of a test chain that finds itself in the opposite phase. This segment has an energy cost of $\sim \chi N_{seg} k_B T$, where N_{seg} is the number of units of the segment. The energy of this incursion will be approximately equal to the current thermal energy of the system, k_BT, which allows the number of units of the segment to be determined, $N_{seg} \sim 1/\chi$. Because the segment of chain still follows Gaussian statistics, the interfacial width is simply $w \sim a\sqrt{N_{seg}}$. From the definition of χ, and the number of molecules per unit area at the interface w/a^3, the interfacial tension is seen to be $\gamma_{AB} = k_BT\sqrt{\chi}/a^2$.

Once the free energy is calculated many details can now be obtained, for example, minimization of Eq. 1.22 with respect to L gives the equilibrium pattern spacing $L \sim \chi^{1/6}N^{2/3}$. This scaling has been verified in numerous experiments, which gives much confidence to the underlying physical idea - the spacing is set by the competition between stretching and interfacial area [33, 34]. However, the strong segregation limit is, only one extreme and is only asymptotically applicable as the chains become infinitely long. Most chains used in industry are much shorter than this, which means another approach must be taken.

To move forward one must consider why the strong segregation assumption fails for shorter chains. If one considers a chain as it moves from disordered to weakly ordered to strongly ordered it becomes clear that the width of the interface changes. In the strongly segregated regime the interface is assumed to be extremely narrow, molecules cannot significantly move into the opposite phase. However, in the disordered state

there is no cost to move into the opposite phase. Clearly in the weak regime the cost of an 'incursion' into the opposite phase is somewhere between the two extremes. Hence, a weak segregation theory must allow for diffuse interfaces between A and B (i.e. $w \rightarrow L$).

Leibler proposed a mean field theory of the weakly segregated state that has correctly approximated this diffuse boundary [35]. The full calculation is beyond the scope of this introduction and will not be given here, however a discussion of the main results of this important contribution is certainly worthwhile. Leibler's derivation begins by identifying the average deviation of the A monomer density from that of the homogeneous state, $\phi(r)$, as an order parameter that describes the phase transition from the ordered to the disordered state. A Landau expansion [36] was then performed resulting in the following free energy,

$$F = F_0 + k_B T \sum_{n=2}^{\infty} V^{-n} \frac{1}{n!} \sum_{\vec{q_1},\ldots,\vec{q_n}} \Gamma_n(\vec{q_1},\ldots,\vec{q_n})\phi(\vec{q_1})\ldots\phi(\vec{q_n}); \qquad (1.23)$$

where $\vec{q}$ is a wavevector in Fourier space, V is the system volume, and the Γ's are related to the monomer density correlation functions. The correlation functions were calculated with the random phase approximation [35, 37].

Once the free energy has been derived in this manner one can make several important observations. Firstly, the underlying phase pattern can be considered to be built up of many different Fourier modes. More importantly, near the transition one particular wavelength dominates the system and it is this wavelength that mainly sets the scale of the phase separated state (L). This also reveals the proper description of the diffuse boundary between A and B domains, ϕ is a sinusoidal function along the pattern axis and the interface becomes quite wide. Secondly, as the free energy is already expanded in powers of ϕ, we see quite clearly that the transition is first order everywhere along the boundary except when the molecule is symmetric (as the third order term is in general non-zero) [35]. In the symmetric case, the third order term becomes zero, and the transition becomes second order. This preserves much of the analogy between a binary mixture and a diblock copolymer melt because of the analogy with the Cahn-Hillard treatment [38]. Finally the phase stability is easily

determined near the ODT through the assumption of one dominant q, which allows the spinodal to easily be located and a phase diagram can be constructed. An important prediction that will be useful later is that a symmetric diblock copolymer has a spinodal point predicted to be $(\chi N)_{ODT} = 10.495$ (compared with 2 in the binary blend).

This theory, while immensely successful in describing the phase of a diblock copolymer melt, also suffers from several drawbacks. Primarily, Leibler's theory is confined to a small range of applicability around the order disorder transition point. This is similar to the shortcomings of the theory of the strong segregation regime, in that it explores one of the two extremes of ordered state along the continuum from weakly segregated to strongly segregated. Furthermore, this method is only approximate; it is ultimately a truncated series. Finally Leibler's theory ignores fluctuations of the mean field which are a major contribution to the state of the system near the ODT.

Self-consistent field theory (SCFT) provides an alternative which successfully connects both the weak and strong segregation regimes, as well as providing an exact solution to the mean field theory [7, 25, 39–42]. Although the complexity of this theory precludes a detailed discussion, some comments are necessary. The technique begins with the assumption of some background field due to the average contribution of nearby chains. This field is then used to predict the energies of the different possible molecular conformations of a test chain. The conformations can then be used to recalculate the field which we began with. After much iteration the result narrows in on the appropriate monomer density and free energy. With this numerical free energy many of the same details calculated with Leibler's theory and the strongly segregated theory can be found [41]. While immensely successful SCFT also has some drawbacks, for example, its numerical complexity. There are also no fluctuation considerations in the theory, and it therefore locates the phase boundaries incorrectly as does Leibler's theory.

In summary, diblock copolymers are polymer molecules of amphiphillic nature that microphase separate into intricate ordered structures. These structures can be understood with the help of different approximate theories, or with the exact SCFT. Despite several decades of intense research, there remain several challenges. This

includes an understanding of the dynamical processes involved in anisotropic liquids such as diblock copolymers, and most deeply, how fluctuations alter the nature and location of the order disorder transition.

Chapter 2

Polymer Droplets

In this chapter we consider the geometry and dynamics of small droplets of liquid on solid substrates. We compare the behavior of homopolymeric fluids with that of symmetric diblock copolymers in order to illustrate the differences caused by the anisotropic nature of the latter.

2.1 Statics

We begin by comparing the measured shape of a droplet of homopolymer with that of a diblock copolymer both above and below the ODT. In so doing we discover a dramatic difference between the two cases. Homopolymeric fluids (as any Newtonian fluid) form spherical caps whereas the diblock copolymers, while still fluid, form nearly conical terraced shapes. Our analysis of this dramatic difference relies on the minimization of a simple free energy function and leads us to a new physical effect - the repulsion of two adjacent lamella edges. We begin with a discussion of homopolymer and disordered block copolymer droplets, and then present the first paper of this thesis in which ordered diblock copolymer droplets are studied.

The details of the molecules used in these studies are reproduced below in Table 2.1. This table, which also appears in the first published work, is reproduced here due to an error in one of the published thickness measurements. This error was due to an improperly calibrated atomic force microscope which has since been corrected.

Table 2.1: Polymer Details - The number averaged molecular weights for the PS and PMMA blocks, the polydispersity index, and the microstructural state at 180 °C.

M_n^{PS}	M_n^{PMMA}	N	Polydispersity	L(measured)	State
10 000	10 000	206	1.05	14.5 ± 0.5	Disordered
12 800	12 900	252	1.05	18.0 ± 0.5	Disordered
14 900	13 100	274	1.05	19.0 ± 0.5	Weakly Ordered
18 000	18 000	353	1.07	26.6 ± 0.5	Ordered
21 000	21 000	412	1.07	28.3 ± 0.5	Ordered
25 000	26 000	500	1.09	30.6 ± 0.5	Ordered

Our measurements are in otherwise perfect agreement with other studies of lamellar thickness [43].

2.1.1 Homopolymer

A droplet of homopolymer on a solid substrate will adopt a shape that minimizes the droplets total free energy. Hence, we begin by defining the free energy of a small parcel of fluid in contact with some rigid boundary (see Fig. 2.1). The energies involved are once again rooted in the molecules that make up the fluid. A fluid molecule surrounded by other fluid molecules will (as discussed earlier) feel an energy proportional to the number of neighbours around it. As a liquid is a condensate, we can safely assume that these interactions are favourable. A molecule at a surface, however, feels less fluid neighbours than does a molecule in the bulk and therefore the interface comes at an increased cost given by the surface tension γ. Calculated on a lattice, the surface tension would be given by $\gamma \sim \chi k_b T / v^{2/3}$; where v is the volume of a lattice site [12]. Most concisely, the fluid adopts a shape that minimizes surfaces.

There are three interfaces in the problem, the solid-vapour, the solid-liquid, and the liquid-vapour. As fluid molecules at each of these surfaces come at an energetic cost compared to molecules in the bulk, an energy must be assigned to each. The shape of the droplet can then easily be determined by minimizing the free energy while keeping the volume constant.

To calculate the shape we begin with the assumption of axial symmetry, which

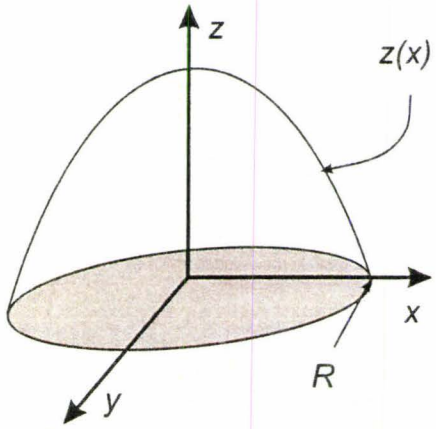

Figure 2.1: Schematic of a droplet of polymer on a solid substrate. The droplet is cylindrically symmetric and has a surface labeled by the curve $z(x)$ which terminates at the surface a distance R from the droplets center.

allows us to write the free energy as

$$F = \gamma_{lv} 2\pi \int_0^R x\sqrt{1+\dot{z}^2}\partial x + (\gamma_{ls} - \gamma_{sv})2\pi \int_0^R x\partial x; \tag{2.1}$$

where γ is the energy of the interface and the subscripts refer to the liquid (l), solid (S) and vapour (v) respectively. R is the point at which the droplet's free surface contacts the substrate. If the volume constraint is written as $V = 2\pi \int_0^R xz\partial x$, then it becomes clear that the shape of the surface can be determined by the usual techniques of variational calculus. That is, the solution of,

$$\frac{\partial F}{\partial z} - \frac{\partial}{\partial x}\frac{\partial F}{\partial z} = 0; \tag{2.2}$$

where $F = \gamma_{lv} x\sqrt{1+\dot{z}^2} - \lambda xz$ and λ is a Lagrange multiplier. Solving this partial differential equation yields

$$z = \sqrt{\frac{\gamma_{lv}^2}{\lambda^2} - x^2} + c; \tag{2.3}$$

with c as an integration constant. Using the volume constraint we find Lagrange multiplier is given by $\lambda = \gamma_{ab}/R$. Finally, the integration constant is set by the balance of surface energies.

Figure 2.2: Water droplets on a tulip. Note the spherical cap shape of each drop.

The main result is the shape predicted by Eq. 2.3. This curve is a sphere centered at $(0, -c)$ - a droplet is a spherical cap. This result is easily verified by the observation of a fluid droplet on a surface (see Fig. 2.2).

This spherical cap shape is also observed in disordered diblock copolymer droplets, as is shown in Fig. 2.3. Here we have annealed a droplet of disordered copolymer for a long time at 180°C under vacuum. The droplet is on an atomically flat substrate (electronics grade silicon) that has been cleaned by super-critical CO_2 and UV-ozone treatment. The topography has been recorded by atomic force microscopy. The spherical nature of these droplets is exactly as we would expect, a disordered diblock copolymer will behave exactly as a homopolymer or Newtonian fluid under these static, equilibrium conditions.

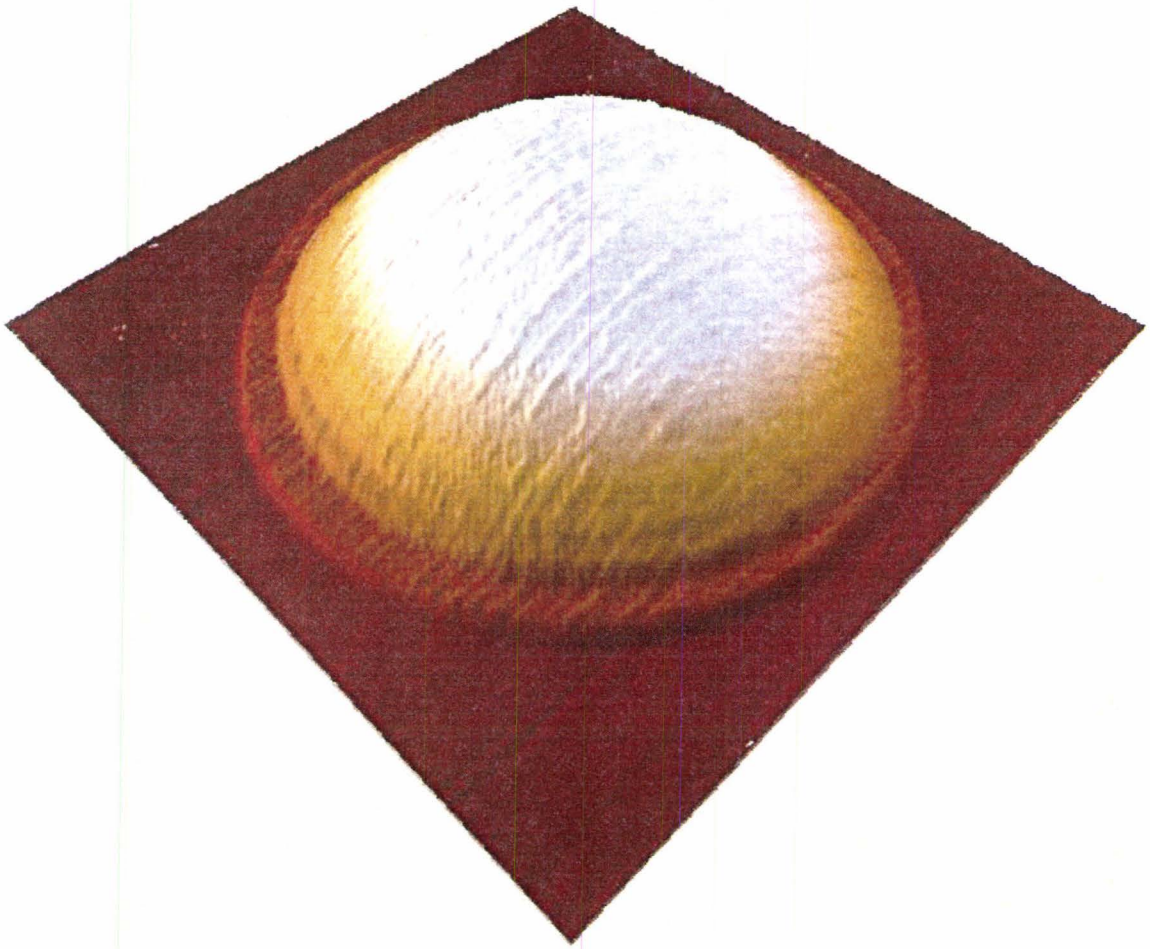

Figure 2.3: A three dimensional rendering of a typical droplet of disordered block copolymer, in this case a molecular weight of 27kg/mol is shown. The image is 10×10 μm and has a z scale of approximately 130 nm. Note the surface induced ording (bumps near the substrate) and wetting monolayer. These two effects are discussed in Section 2.2 and Section 3.2 respectively.

2.1.2 Paper I: Droplet Shape of an Anisotropic Fluid

A.B. Croll, M.V. Massa, M.W. Matsen and K. Dalnoki-Veress, *Phys. Rev. Lett.* **97** 24502 (2006)

In this first published work we have studied the shape formed by small droplets of diblock copolymer by atomic force microscopy. In contrast to the previously discussed spherical solution of an ordinary fluid, here we find nearly conical shapes in ordered diblock copolymer droplets. We model the atypical shape by considering the free-energy of a stack of fluid disks. Minimization of this free energy predicts a cylinder to be the lowest energy shape. Hence, the need for an additional physical mechanism beyond the interfacial tension on the disks was revealed. We considered an edge-edge repulsion term that arises due to the extra stress of a lamellar edge. As the two edges come closer to each other, the stress from each edge is shared in the same location which comes at a higher energetic cost. This additional effect contributed to excellent fits with the droplet measurements.

Deeper theoretical analysis reveals that the shapes predicted by the simple free energy model are in fact hyperbolic caps, a close relative of the spherical cap. This realization allows for the non-invasive experimental classification of droplets. A general quadratic curve can be fit to a drop, and geometry of the curve can tell the observer wether or not a droplet is ordered (hyperbolic) or disordered (spherical). To verify our prediction, we use this new technique to locate the ODT point of the diblock used, and find good agreement with the literature [44].

2.2 Dynamics

The dynamics of spreading droplets also reveal significant differences between ordinary and diblock copolymer fluids. In the case of block copolymers we note a dramatic slowing, which has significant implications to the surface coating industry. We show how this slowing is a direct result of the fluid's rheological character. As such we propose that the simple experiment of watching a droplet of fluid spread on a substrate is effectively an experiment characterizing the rheology of the fluid.

When the droplet topography is observed with the resolution of the atomic force microscope we see a fingering instability of well defined wavelength. We characterize this instability experimentally and provide a state diagram locating the instability for a number of molecular weights. We analyze the fingering in analogy to the mullins-Sekerka instability which governs the intricate pattern formation of the snowflake.

2.2.1 Paper II: Spreading of Symmetric Diblock Copolymer Droplets - A Novel Probe of Polymer Micro-Rheology

A.B. Croll and K. Dalnoki-Veress, *Euro. Phys. J. E.* **Submitted**

In this second work we once again compare ordinary fluid behavior with that of a symmetric diblock copolymer. In this case, we investigate the dynamics of a fluid droplet covering a favourable substrate, a geometry relevant to the paint industry. The experiments are conducted with an optical microscope in combination with an atomic force microscope. We find that the diblock copolymer flows in a similar power law manner to that of ordinary fluid, $R \sim t^m$; where R is the contact radius and t is time. However, we find the exponent, m, to be much lower than predicted for ordinary fluids, leading to an incredibly slow dynamic for spreading diblock droplets. The slowing is a direct result of the polymers internal structure, which we verify by comparing disordered diblock copolymer with ordered diblock copolymer.

This result can be accounted for by proper inclusion of the block copolymer's rheological response in a simple scaling model. In more simple language, one must acknowledge the non-linear viscosity (response to stress) of a block copolymer fluid. Or, in reverse, the flow is a measurement of a fluid's non-linear viscosity. In an ordinary fluid viscosity is a constant independent of the fluid's velocity, in a diblock (and indeed many complex fluids) the viscosity depends on the speed of the fluid flow.

As we study the diblock's viscosity we further reveal that there is no significant molecular weight dependence to the process for the molecular weights studied. This result is very different from the strong dependence of homopolymer viscosity on chain length, and can be attributed to a different mechanism of fluid motion. Homopolymer is free to move in any direction, but lamella never cross. This means that the bulk of block copolymer viscosity is due to lamellar sliding and molecules of each adjacent lamella do not significantly mix. The result is a viscosity that is much more closely related to brush-on-brush friction.

2.2.2 Paper III: Fingering Instability of a Spreading Lamella

A.B. Croll and K. Dalnoki-Veress, *Phys. Rev. Lett.* **In Prep.**

In this paper we discuss a fingering instability that occurs on the front of the wetting monolayer of a diblock copolymer droplet. We measure the instability with AFM and report a morphological progression from very dendritic to cellular patterns as small to large droplets are investigated. As the morphology strongly suggest an analogy to the solidification of metal crystals in the presence of a solute, we proceed to analyse our findings in terms of the Mullins-Sekerka instability.

By assuming the strong segregation limit for the wetting monolayer, we find fair scaling agreement with the predictions of the linear stability analysis. In particular, because the motion of the front is diffusive, we predict the spacing of the fingers increases as the square root of the wetting front in a sample annealed for a particular time. This also coincides with the morphological progression observed in a sample, slower speeds (smaller droplets) form more dendritic structures, in direct analogy to the solidification of metal blends.

Our simple scaling analysis predicts a weak molecular weight dependence of the fingering wavelength. This prediction is also found to be consistent with measurements. We finish our discussion by presenting the molecular weight dependence of the onset of the instability.

Chapter 3

Thin Films

Just as the surface and internal energies of a droplet of diblock copolymer combine to yield dramatic non-classical static and dynamic behavior, when confined to a thin film diblock copolymers can also show a number of interesting physical phenomena [5,45]. In this chapter we present two related studies of block copolymer thin films. In the first we measure the thickness of lamellar layers and, noting no deviation from bulk spacing, discuss how to use the layer thickness to measure the Flory-Huggins parameter. This system also allows for a simple method to measure the anisotropic diffusion of these molecules. These simple measurements could easily be adapted to many other lamella forming systems.

In the second study we observe the surface induced ordering in a similarly simple way. Here we use an optical microscope to observe step edges in a gradient thickness film of diblock copolymer near the ODT. These films show order in a number of layers near the substrate despite being above the bulk ordering temperature. Our hands-free method allows high-resolution observation of the shape of the divergence of the correlation length as the ODT is approached. We also have access to dynamical information on the ordering and disordering in the system. This shows a disordering time that is significantly faster than the ordering time, something that has direct implications on what true equilibrium means in a thin block copolymer film.

Finally we add some comments on how these studies are easily verified by exploiting an alternate parameter (N in the place of T). Here we reproduce certain aspects

of the above two thin film studies with a second set of samples (PS-PMMA instead of PS-P2VP). This allows us great confidence in the techniques that we develop in these thin film studies, and is the beginning of a very good set of ODT measurements for theoretical considerations. Both studies indicate an ODT of ~ 18, which is in-line with current theoretical models; however, numerical agreement is still beyond our grasp.

3.1 Paper IV: Kinetics of Layer-Hopping in a Diblock Copolymer Lamellar Phase

A.B. Croll, A.-C Shi, M.W. Matsen and K. Dalnoki-Veress, *Euro. Phys. J. E* **27** 407 (2008)

This work shows a very simple method of observation of changes in diblock copolymer lamellar thickness using an optical microscope. This experiment, coupled with the accurate SCFT prediction of lamellar thickness, leads to the measurement of the Flory-Huggins interaction parameter with unpresidented simplicity and accuracy. We verify our technique by measuring a well known polymer and comparing the value of χ obtained with our optical method and that of more complex neutron scattering measurements. The result of this comparison reveals several important details: 1. Our trivial measurement is *at least* as good as highly complex scattering methods; 2. Our measurement verifies the quantitative predictions of SCFT.

Our optical method also allows us to measure the diffusion of diblock-copolymer in the direction perpendicular to the lamella. In order to diffuse in the perpendicular direction, one block, A, must pass through the B-rich phase. This corresponds to a slow barrier-hopping process, which we can measure directly and without any mixing of the parallel diffusion signal. We show, for the first time, that this barrier can be entirely accounted for with the predictions of SCFT.

3.2 Paper V: Ordering of a Lamella Forming Fluid Near an Interface.

A.B. Croll, A.-C Shi and K. Dalnoki-Veress, *Phys. Rev. Lett.* **Submitted**

In the final work presented in this thesis we conduct experiments on thin 'wedge' films of diblock copolymer. A 'wedge' is simply a thin film that has a gradient in thickness from one side of a sample to another. When allowed to order, a 'wedge' film of symmetric diblock copolymer forms several discrete terraces due to the lamellar structure of the fluid, which form parallel to the substrate. We observe the edges of each lamella with dark-field optical microscopy and AFM. This allows the direct and non-invasive observation of the dynamics of ordering in a thin block copolymer film as it traverses the ODT.

We begin by studying the surface induced ordering of a sample (that is, order induced in an otherwise disordered sample simply by the presence of a surface). We observe this well-known effect at very high resolution which reveals a curious deviation from the predicted scaling at very low thicknesses ($\sim 3 layers$) or high temperatures ($\sim T_{ODT} + 50\text{K}$) [6]. The scaling of the higher thickness region, when combined with our earlier measurement of χ, locates the ODT at $\chi N = 18$. This high value cannot currently be reconsiled with the predictions of any theory.

Beyond these observations, our new method allows the dynamics of the ordering and disordering process to be tracked one layer at a time. We find that the disordering timescale is independent of quench depth (temperature jump). This is because the relaxation is dominated by viscous processes. The ordering is found to be quite different; it has a timescale that depends exponentially on the distance of the layer from the substrate. This timescale can be understood by analogy to the Cahn-Hillard equation of a simple binary blend - the layer forms by a spontaneous process analogous to spinodal decomposition. In the case of a diblock copolymer, this simple analogy is modified by the molecular connectivity as recently shown theoretically by Yamada et. al. [46].

3.3 Additional Studies

The two previous studies have both used a polymer that has a very high degree of sensitivity to temperature changes (which is reflected in the Flory-Huggins parameter). Indeed the temperature sensitivity was exploited in both studies in order to perform the measurements necessary to determine χ and $(\chi N)_{ODT}$. There is, of course, an alternative mechanism that can be exploited in studies of block copolymer phase. The molecular weight can be changed and in much the same way both χ and $(\chi N)_{ODT}$ can be located. In order to provide further confidence in these new techniques we provide these alternative measurements using a different polymer which has a much lower temperature dependence.

Samples were prepared by dusting freeze-dried polystyrene-b-poly(methyl methacrylate) onto silicon substrates that have been cleaned by super-critical CO_2 and UV-Ozone treatment. Samples were then annealed for long times at 190°C, yielding droplets as described in chapter 2. Several different molecular weights were used, the details of which appear in table 2.1. Lamellar thickness is a non-linear, increasing function of N as can be seen in Fig. 3.1.

Eqn. 2 of the fourth paper presented above, can be fit to this data yielding a measurement of the one free parameter $\chi = 0.068 \pm .005$. This is notably larger than the values measured by Russell et.al. in [44] (at 180°C they find $\chi = 0.037$). This difference is not unexpected, as Russell et. al. rely on the scattering function derived by Leibler in [35] which is not corrected for fluctuation effects. In fact, by using the fluctuation corrected scattering function proposed by Fredrickson and Helfand in [47] one finds that the Russell data is well fit with $\chi = 0.061 \pm .002$. This is much closer to our measurement which needs no external manipulation to account for fluctuation effects as they are not expected to alter lamellar thickness [8]. We also note that the fluctuation correction proposed by Fredrickson and Helfand is still just a modification to the approximate theory of Leibler, and is therefore not expected to be quantitatively accurate.

We have also located the ODT in this set of diblock samples by the method described in section 2. In this study we noted the sample at $N = 288$ to be ordered,

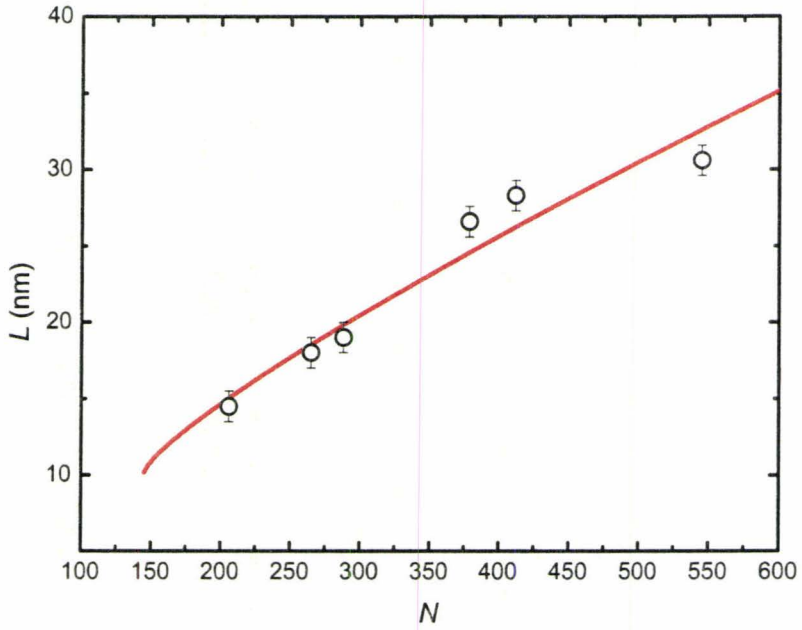

Figure 3.1: Thickness of various PS-PMMA samples as a function of N. The curve is a fit to Eqn. 2 of paper four and yields $\chi = 0.0685 \pm .005$

but only weakly at 190°C, while the sample at $N = 265$ is distinctly disordered in the bulk. Hence we shall take $N_{ODT} \simeq 270 \pm 10$, where the error indicates the significant uncertainty in this measurement. This highlights the usefullness of the high resolution achieved in our earlier study (section 3.2). Combining these two measurements we locate the order to disorder point at $(\chi N)_{ODT} = 18.5 \pm 2$.

Combined with our earlier study of PS-P2VP where we found $(\chi N)_{ODT} = 18.0 \pm 0.1$ this second measurement strongly suggests that the spinodal point is located considerably higher than the SCFT and weak segregation theory prediction of 10.495. The reason for this high value of the spinodal point is well known to be a fluctuation effect, but its exact value has not yet been successfully predicted [8,47]. For example, Fredrickson and Helfand predict a value given by

$$(\chi N)_{ODT} = 10.495 + 41.0\bar{N}^{1/3} \tag{3.1}$$

where $\bar{N} = a^6\rho^2 N$ and a is the statistical segment length and ρ is the density. This suggests that $a^3\rho$ is always very close to one, which is not very realistic given the

variance in these parameters from one polymer to another. Other predictions using Monte-Carlo methods give $(\chi N)_{ODT} \sim 28$ which is certainly outside of the range of our measurements [8].

This study of PS-PMMA lamellar thickness and ODT point, and our previous PS-P2VP study, provide the starting point of an important set of data for theoretical analysis. These two studies rely on minimal assumption, or data analysis, and therefore have a much lower possibility of error in interpretation. This provides a very reliable set of experimental data (and techniques to study other molecules) that can be used to test theoretical models of fluctuations in diblock copolymer melts near the order disorder transition.

Chapter 4

Conclusions

In this thesis we have presented the results of several studies of the behavior of diblock copolymer fluids. We began by exploring the consequences of the competition of two length scales (the internal lamellar structure and the mesoscopic droplet) on the static and dynamic behavior of the system. We noted a significant departure from the behavior of isotropic fluids - most notably that the droplets of block copolymer form nearly conical equilibrium shapes. We also explored how having molecules confined to exist within a lamella dramatically impeded the ability of the droplets to flow and cover a surface. Finally we explored a curious fingering instability of the surface monolayer as its constituent molecules diffused across the surface.

In a second set of works, we considered the behavior of the block copolymer molecules in an alternate geometry - confinement to a thin film. We first noted that the combination of the fact that the equilibrium lamellar spacing is directly related to the temperature and that a thin film will form discrete surface domains with material in excess of a complete layer to measure the Flory-Huggins parameter with an optical microscope. This technique has far reaching possibilities due to its simplicity, and universality. For example, any researcher with an optical microscope can now determine the most fundamental parameter characterizing diblock copolymer behavior. We also show how these domains can be used to examine the diffusion of block copolymers from one lamellar layer to another; an experiment that we feel has implications for any lamella forming system.

We also use thin film 'wedge' samples to observe how an attractive substrate causes the block copolymers to order near the surface despite their being in the bulk disordered state. We find remarkable agreement with the scaling of Fredrickson's predictions, and use this scaling to make a high resolution measurement of the location of the ODT [6]. We can also use the 'wedge' samples to observe directly the dynamics of disordering and of ordering of these fluids. We finish this section by repeating these two works with a second polymer and the alternative variable (varying N in the place of T). The agreement of our ideas and the existing literature confirm the validity of these new techniques. The two measurements of the ODT point also form the beginning of an excellent set of data to test theoretical predictions of fluctuation effects or other factors influencing the location of the ODT.

These various studies illustrate how pattern formation and simple, creative experiments can reveal interesting fundamental details of diblock copolymer melts. The avoidance of significant theoretical complexity and the high resolution of our experiments allow us to see clearly the successes of modern theory such as SCFT, as well as its limitations (for example in predicting the exact location of the ODT). This clearly illustrates the road towards our future understanding of these complex materials.

Bibliography

[1] de Gennes, P. G., *Soft Interfaces: The 1994 Dirac Memorial Lecture*, Cambridge University Press, 1997.

[2] Black, C. et al., IBM J. Res. Dev. **51** (2007) 605.

[3] Dai, K. H., Kramer, E. J., and Shull, K. R., Macromolecules **25** (1992) 220.

[4] Langer, J. S., Rev. Mod. Phys. **52** (1980) 1.

[5] Anastasiadas, S. H., Russell, T. P., Satija, S. K., and Majkrzak, C. F., Phys. Rev. lett. **62** (1989) 1852.

[6] Fredrickson, G. H., Macromolecules **20** (1987) 2535.

[7] Shull, K. R., Macromolecules **25** (1992) 2122.

[8] Vassiliev, O. N. and Matsen, M. W., J. Chem. Phys. **118** (2003) 7700.

[9] Strobl, G., *The Physics of Polymers, 2nd Edition*, Springer-Verlag, 1997.

[10] de Gennes, P. G., *Scaling Concepts in Polymer Physics*, Cambridge University Press, 1997.

[11] Jones, R. and Richards, R., *Polymers at Surfaces and Interfaces*, Cambridge University Press, 1999.

[12] Jones, R. A. L., *Soft Condensed Matter*, Oxford University Press, 2002.

[13] Rudnick, J. and Gaspari, G., *Elements of the Random Walk: An Introduction for Advanced Students and Researchers*, Cambridge University Press, 2004.

[14] Reichl, L., *A Modern Course in Statistical Physics, 2nd Edition*, John Wiley and Sons, Inc., 1998.

[15] Creton, C., Kramer, E., Brown, H., and Hui, C.-Y., Adv. Poly. Sci. **156** (2001) 53.

[16] Bray, A., Phys. Rev. Lett. **62** (1989) 2841.

[17] de Gennes, P., J. Chem. Phys. **72** (1980) 4756.

[18] Flory, P., J. Chem. Phys. **10** (1942) 51.

[19] Huggins, M., J. Phys. Chem. **46** (1942) 151.

[20] Huggins, M., J. Am. Chem. Soc. **64** (1942) 1712.

[21] Maurer, W. et al., J. Chem. Phys. **108** (1998) 2989.

[22] Dudowicz, J. and Freed, K., macromolecules **24** (1991) 5076.

[23] Cahn, J. W., J. Chem. Phys. **42** (1965) 93.

[24] Bates, F. S. and Fredrickson, G. H., Annu. Rev. Phys. Chem. **41** (1990) 525.

[25] Matsen, M., J. Phys.: Condens. Matter **14** (2002) R21.

[26] Discher, D. E. and Eisenberg, A., Science **297** (2002) 967.

[27] Fredrickson, G. H. and Bates, F. S., Annu. Rev. Mater. Sci. **26** (1996) 501.

[28] Matsen, M. and Schick, M., Phys. Rev. Lett. **72** (1994) 2660.

[29] Helfand, E., J. Chem. Phys. **62** (1975) 999.

[30] Semenov, A. N., Sov. Phys. JETP **61** (1985) 733.

[31] Ohta, T. and Kawasaki, K., macromolecules **19** (1986) 2621.

[32] Semenov, A., Macromolecules **26** (1993) 6617.

[33] Hashimoto, T., Shibayama, M., and Kawai, H., Macromolecules **13** (1980) 1237.

[34] Hasegawa, H., Tanaka, H., Yamasaki, K., and Hashimoto, T., Macromolecules **20** (1987) 1651.

[35] Leibler, L., Macromolecules **13** (1980) 1602.

[36] Landau, L., Phys. Z. Sov. **11** (1937) 545.

[37] de Gennes, P., J. De Phys. **31** (1970) 235.

[38] Bates, F. S., Science **251** (1991) 898.

[39] Helfand, E., Macromolecules **8** (1975) 552.

[40] Helfand, E., J. Chem. Phys. **62** (1975) 999.

[41] Matsen, M. W. and Bates, F. S., macromolecules **29** (1996) 1091.

[42] Shi, A. C., Noolandi, J., and Desai, R., Macromolecules **29** (1996) 6487.

[43] Sivaniah, E. et al., Macromolecules **41** (2008) 2584.

[44] Russell, T. P., R. P. Hjelm, J., and Seeger, P., Macromolecules **23** (1990) 890.

[45] Fasolka, M. J. and Mayes, A. M., Annu. Rev. Mater. Res. **31** (2001) 323.

[46] Yamada, K., Nonomura, M., and Ohta, T., macromolecules **37** (2004) 5762.

[47] Fredrickson, G. H. and Helfand, E., J. Chem. Phys. **87** (1987) 697.

Appendicies

Appendix A: Published Works

I. A.B. Croll, M.V. Massa, M.W. Matsen and K. Dalnoki-Veress, Droplet Shape of an Anisotropic Fluid. *Phys. Rev. Lett.* **97** 24502 (2006)

II. A.B. Croll and K. Dalnoki-Veress, Spreading of Symmetric Diblock Copolymer Droplets - A Novel Probe of Polymer Micro-Rheology. *Euro. Phys. J. E.* **Submitted**

III. A.B. Croll and K. Dalnoki-Veress, Fingering Instability of a Spreading Lamella. *Phys. Rev. Lett.* **In Prep.**

IV. A.B. Croll, A.-C Shi, M.W. Matsen and K. Dalnoki-Veress, Kinetics of Layer-Hopping in a Diblock Copolymer Lamellar Phase. *Euro. Phys. J. E* **27** 407 (2008)

V. A.B. Croll, A,-C Shi and K. Dalnoki-Veress, Ordering of a Lamella Forming Fluid Near an Interface. *Phys. Rev. Lett.* **Submitted**

Appendix B: works not included in thesis

I. A.B. Croll, M.H. Müsser, and K. Dalnoki-Veress, Friction Measurements with Dewetted Polymer Droplets. *In Preparation*

II. A.B. Croll, and K. Dalnoki-Veress, Hole Nucleation and the Stability of Symmetric Diblock Copolymer Films, *In Preparation*

III. A.B. Croll, M.J. Farrar, and K. Dalnoki-Veress, The Effects of Lamellar Confinement on Hole Growth in Free-Standing Polymer Films. *In Preparation*

IV. J. Parete, A.B. Croll, A.-C Shi, and K. Dalnoki-Veress, Directed Pattern Formation in Locally Heated Diblock Copolymer. *In Preparation*

V. A.B. Croll, A.-C Shi, K. Dalnoki-Veress, and M.W. Matsen, Block Copolymer Lamella: Simple Experiments and Complex Physics. *PIC PAC* **64**, 126.

PHYSICAL REVIEW LETTERS

Articles published week ending
17 NOVEMBER 2006

Volume 97, Number 20

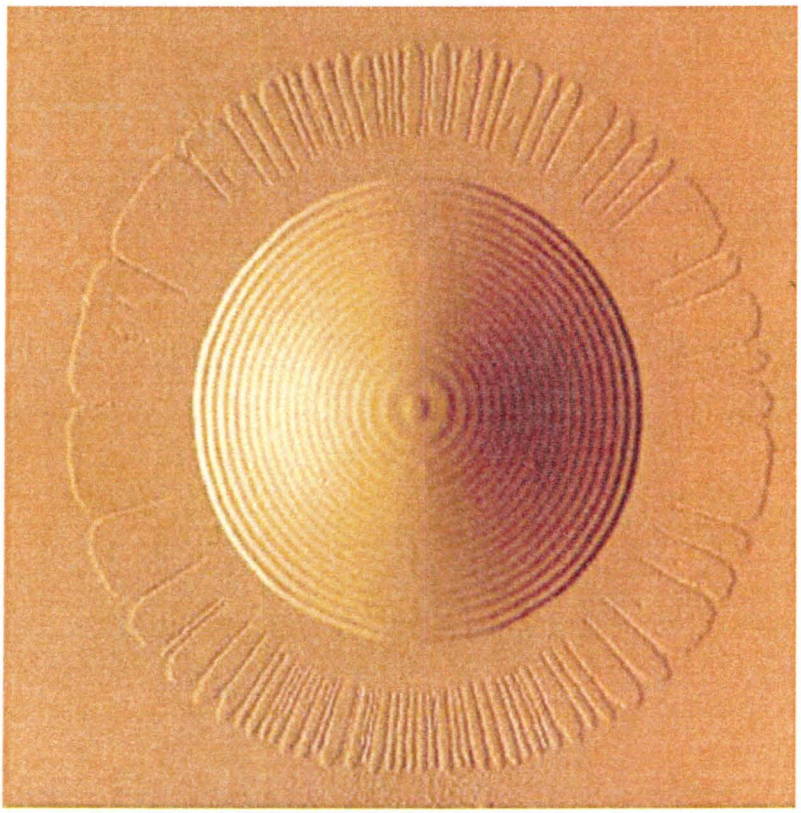

APS physics

Published by The American Physical Society

Droplet Shape of an Anisotropic Liquid

Andrew B. Croll,[1] Michael V. Massa,[1] Mark W. Matsen,[2] and Kari Dalnoki-Veress[1,*]

[1]*Department of Physics & Astronomy and the Brockhouse Institute for Materials Research, McMaster University, Hamilton, ON, Canada*

[2]*Department of Mathematics, University of Reading, Whiteknights, Reading, United Kingdom*

(Received 2 June 2006; published 17 November 2006)

We investigate how a droplet of a complex liquid is modified by its internal nanoscale structure. As the liquid passes from an isotropic disordered state to an anisotropic layered morphology, the droplet shape switches from a smooth spherical cap to a terraced hyperbolic profile, which can be modeled as a stack of thin concentric circular disks with a repulsion between adjacent disk edges. Our ability to resolve the detailed shape of these defect-free droplets offers a unique opportunity to explore the underlying physics.

DOI: 10.1103/PhysRevLett.97.204502 PACS numbers: 47.20.Hw, 61.25.Hq, 68.03.Cd, 68.08.Bc

Consider a simple fluid droplet on a solid substrate. In the absence of gravity or for small droplets, the shape is governed by the surface tension requirement of a minimal area and results in a spherical cap. The *contact angle* (the angle between the liquid-air and liquid-substrate interface at the three-phase contact line) depends on the three interfacial tensions in the system according to Young's equation [1]. Droplets of rain on a leaf are a familiar example and can be particularly striking in the case of *superhydrophobic* surfaces (with very high contact angles) like a lotus leaf [2,3]. The simple picture of a spherical droplet becomes more complex in the case of an anisotropic liquid [4], where there is some underlying order or on substrates with some lateral order [5]. Here we show that, when diblock copolymers form an ordered liquid with a lamellar structure, droplets are found to exhibit a *hyperbolic* shape. This unusual droplet shape, which can be understood from a simple model, switches to a spherical cap once the ordered structure is lost (i.e., upon passing through the order-disorder transition). While deviations from a spherical droplet are of general fundamental interest, there is also great technological potential given that the hyperbolic shape is highly regular, controllable, and switchable. Furthermore, the wide variety of existing block-copolymer nanostructures [6] implies a rich assortment of possible droplet shapes, all of which could be utilized as building blocks for nanotechnology.

Diblock copolymers are long chain molecules comprised of two chemically distinct parts (i.e., blocks) covalently bonded together. The general chemical incompatibility of the two components imparts the molecules with amphiphilic behavior that drives them to self-assemble into ordered nanostructures, where the unlike blocks reside in separate domains. The connectivity of the blocks limits the length scale of the domains to that of the molecules (~ 10 nm), and a complex interplay between the internal interfacial tension and chain stretching causes the domains to adopt morphologies with long-range periodic order. The geometry of the morphology transforms from lamellar to gyroid to cylindrical to spherical as the ratio of the block lengths deviates from one [6–8]. Although the unlike blocks are confined to separate domains, they still maintain liquidlike mobility and thus can be classified as a structured fluid. However, the melt transforms to an amorphous liquid when the temperature is increased above the order-disorder transition (ODT), where entropy dominates the energetic benefits of nanophase separation. Alternatively, the disordered state can be brought about by reducing the molecular weight (M_w) of the molecules, because the energy cost of removing a block from its preferred domain is proportional to its size.

During the last few decades there has been significant effort to study diblocks at surfaces and interfaces [8–20]. This focus is in large part due to fundamental interest in the interdependence of surfaces or interfaces and nanostructure but it is also motivated by the technological importance of self-assembling nanostructures. Potential applications can be found in enhancing material properties, patterning, photonics, lab-on-a-chip devices, information storage, and many others, provided one can control morphology and also the orientation of morphologies (see, for example, ordering by solvent evaporation [21], ordering by substrate topography [22], and ordering by electric fields [23,24]). Understanding wetting/dewetting of diblock copolymers on a substrate is paramount to the coupling of pattern formation on two different length scales: those of dewetting ($\sim 10\ \mu$m) and nanophase separation (~ 10 nm) [14–20]. It was first suggested by Fredrickson that due to the preferential interaction of an interface with one of the blocks there could be induced ordering at the substrate interface even above ODT [9]. Recent experimental work on ordering in thin films above ODT have been carried out by Green and co-workers [20]. In the cases where there is a stronger affinity for one of the blocks and the substrate, a symmetric diblock will form lamellae which order parallel to the substrate, thereby minimizing the interfacial energy.

Typically fluids that do not wet a substrate form spherical cap droplets. However, the shape of nonequilibrium droplets as they are spreading on the substrate can deviate

from the simple spherical cap. In experiments on simple fluids [25] and liquid crystals [26], as well as molecular dynamics on short chain molecules [27] it was found that the spreading droplet can be terraced. Equilibrium droplets which exhibit no flow can also show terracing, but as a result of an underlying anisotropy in a complex fluid like liquid crystals and block copolymers [10,14,28–30]. We find that droplets of symmetric diblock copolymer self-assemble into stacks of concentric circular disks with decreasing radii, again forming terraced profiles. However, we focus on the overall profile of the droplets, similar to previous work on smectic liquid crystal droplets [4]. The relative ease of imaging the terraces of diblock droplets contrasts with liquid crystal droplets where uncertainty about the actual nanostructure and nonequilibrium effects provide further challenges [30]. The droplet profiles we observe are *not* spherical, but a nearly conical shape, which can be understood from a simple model and is described by a hyperbola. Interestingly, the profiles revert to a spherical shape, when the diblock melt loses its internal lamellar structure as M_w is reduced or temperature is increased beyond the ODT.

The polymer used in this work is symmetric monodisperse poly(styrene-methyl methacrylate) (PS-PMMA) obtained from Polymer Source (Dorval, Quebec). The range of total (sum of both blocks) number-averaged molecular weights extends from $M_n = 21$ to 104 kg/mol (see Table I), and spans both sides of the bulk ODT [31]. The substrates were electronic grade Si wafers with the native oxide layer present, which were cleaned by supercritical CO_2 (Applied Surface Technologies) and UV-Ozone in order to remove surface contaminants. The polymer was "dusted" onto the clean Si and then annealed at 180 °C under vacuum ($\sim 10^{-6}$ Torr) for long times (~ 100 h). Annealing well above the glass transition temperature ($\approx$ 100 °C) of both polymer blocks ensures that the polymer can nanophase separate and reach an equilibrium droplet shape. Droplet morphologies were obtained with atomic force microscopy (AFM) in tapping mode. Both topographic and error signal images were collected. The error signal, roughly the derivative of the topography, was used to highlight the edges of lamella. Each step of the terrace is a diblock bilayer arranged *A-B/B-A* in order to minimize the interfacial tension of the system. For the PS-PMMA system the PMMA block has a greater affinity for the substrate and wets the substrate, while the PS block has a lower surface tension (a condition termed asymmetric wetting [8,20]). The minimum in the free energy of the system is obtained with a half lamella (diblock monolayer) at the substrate followed by full lamellae (diblock bilayers) forming the sequence: Si/PMMA-PS/PS-PMMA PMMA-PS/etc. Lamellar heights, L, of the diblock bilayer were measured with AFM and found to be in good agreement with expected values (see Table I) [7,31].

TABLE I. Molecular weights M_n, polydispersity index PI, and lamellar thickness L of the diblocks used.

M_n(PS) (kg/mol)	M_n(PMMA) (kg/mol)	PI	L (nm)
10.5	10.5	1.05	14.6 ± 0.8
13.4	13.6	1.05	18.0 ± 0.4
15.6	13.8	1.05	19.0 ± 2.0
19.3	19.3	1.07	21.6 ± 1.4
27.3	28.3	1.09	27.0 ± 1.2
52.0	52.0	1.09	62.0 ± 3.0

Figure 1 shows an AFM image of the error signal of a PS-PMMA(29.4 k) diblock droplet (the *total* M_n of the diblock is indicated in brackets). The image reveals several important features. (1) The terracing is very clear, and each step corresponds to a diblock bilayer. (2) The rings are almost equally spaced, indicating that the droplet has a nearly conical shape, in contrast with the usual spherical cap. (3) The first layer of the droplet is a monolayer and spreads beyond the base of the bulk of the droplet. The monolayer exhibits a clear fingering pattern. (4) The near perfect circularity of the disks strongly implies that the disks are in equilibrium.

The monolayer can be treated separately. It exhibits slow continuous growth driven by the strong tendency for

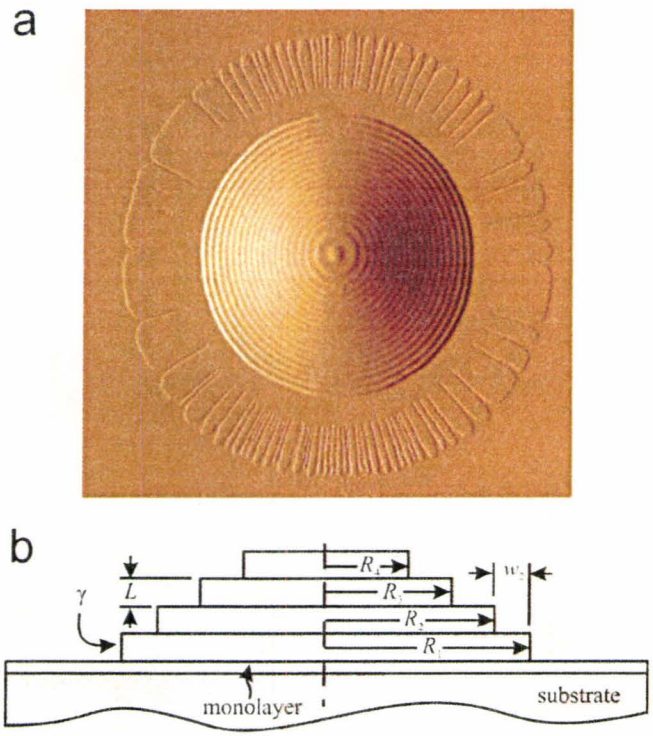

FIG. 1 (color). (a) Atomic force microscopy error signal. In this 32 × 32 μm scan of a diblock droplet PS-PMMA(29.4 k), each ring corresponds to one lamella (diblock bilayer). The droplet has the morphology of a stack of concentric disks with increasing diameter towards the substrate. We note that the error signal tracks vertical fingers faithfully. The lack of detail in the horizontal fingers is due to the horizontal scan direction, and the sensitivity of the signal to *changes* in height. (b) Schematic of an ordered droplet denoting the relevant parameters: bilayer thickness L, disk radii R_i, edge tension γ, and terrace widths w_i.

PMMA to wet the substrate, with the bulk of the droplet acting as the reservoir from which it acquires new material. The fingering pattern is complex and dependent on both the temperature at which the sample is annealed as well as the M_w and will be the subject of a further publication. Because the monolayer spreads very slowly in comparison with the time scale on which the droplet shape is established (the time scales differ by more than 2 orders of magnitude), we can consider the bulk of the droplet to be in equilibrium on a static monolayer brush. Ultimately, if one waits a sufficient number of days, the monolayer will spread to such an extent so as to consume the entire droplet, since the minimum energy state is to cover the entire substrate with a layer of PMMA.

The behavior of the bilayers can be understood in terms of the simple model depicted in Fig. 1. This model assumes that the monolayer forms a relatively static PS surface, upon which n bilayers adjust their respective radii, R_i, so as to minimize their total free energy,

$$\frac{F}{2\pi} = \gamma \sum_{i=1}^{n} R_i + \sum_{i=2}^{n} R_i U(w_i).$$

The PS-air tension of the horizontal surfaces (including that of the monolayer carpet) is omitted because their combined area remains fixed. The only variation in area occurs due to the vertical steps; this part of the PS-air surface energy is combined in γ along with all the other energy costs of forming an edge to the bilayer. The last term of the free energy represents a repulsion between adjacent edges and depends on the terrace width $w_i = R_{i-1} - R_i$. The source of the repulsion is conceptually simple. Of course, the terraces will not exhibit the sharp idealized steps depicted in Fig. 1(b). Their equilibrium shape will be dictated by a competition between the air-PS tension, which tends to smooth out sharp corners, and the effective elasticity of the bilayers, which favors a uniform thickness [7]. For large isolated terraces, this competition will select a preferred profile with some characteristic length scale over which the bilayer disk acquires its preferred uniform thickness, L. When the separation between terraces, w_i, becomes less than this length scale, their shapes will be forced to deviate from the preferred profile causing a rise in the free energy. This excess energy represents the effective interaction, $U(w_i)$, responsible for the edge-edge repulsion. We find that the droplet shape is not particularly sensitive to the details of this repulsion, and choose the simple form $U(w_i) = U_0 \exp(-w_i/w_0)$, where U_0 and w_0 are fitting parameters. Naturally, the free energy must be minimized with respect to n and the R_i under the constraint that the total volume, $V = \pi L \sum_{i=1}^{n} R_i^2$, of the droplet remains fixed. We search for the equilibrium droplet shape by stepping through each value of n and introducing a Lagrange multiplier (i.e., pressure), P, which allows us to minimize $\Omega = F - PV$ with respect to R_i as if there is no constraint.

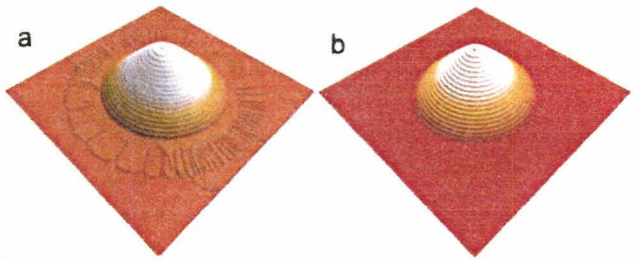

FIG. 2 (color). (a) Three-dimensional rendering of the diblock droplet shown in Fig. 1. The droplet has a diameter of 17.6 μm. (b) The output of a best fit of the model to the data. To facilitate comparison, the same surface rendering is used.

In Fig. 2 we show AFM topography data as well as a best fit of the model to the data (the parameters $L = 19.0$ nm, $V = L1.68 \times 10^4$ μm^2, and $R_1 = 8.78$ μm, are fixed to their experimentally determined values. The fitting parameters are $w_0/L = 1$ and $U_0/\gamma = 1.1 \times 10^6$). The model is in very good agreement with the data and seems to capture all the essential physics. Numerically the location of the edges predicted by the model fall *exactly* on a hyperbola. Hence, droplets of an anisotropic fluid of this type form a hyperbolic cap, rather than the spherical cap for an isotropic fluid. This is very clear in Fig. 3 where a circle and hyperbola are fit to a droplet in the disordered and ordered state. As first predicted by Fredrickson [9], we also observe some ordering induced by the substrate for temperatures above ODT as can be seen as a small step at the droplet base in Fig. 3(a). To differentiate between the ordered and disordered droplet in a quantitative manner, the profile can be fit to the generic equation $0 = Ax^2 + Bxy + Cy^2 + Dx + Ey + F$. If the droplet is a spherical cap, the discriminant, $\Delta = B^2 - 4AC < 0$, while for a hyperbolic $\Delta > 0$. Measurements at 180 °C were carried

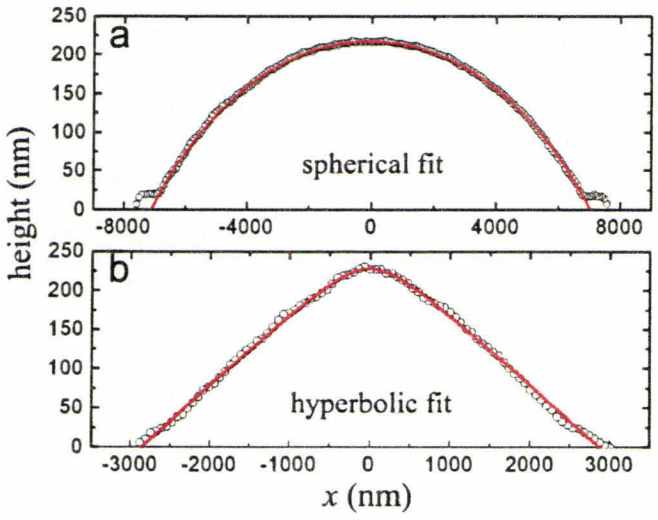

FIG. 3 (color online). Droplet profiles in the amorphous and ordered state. (a) AFM profile and fit to an amorphous spherical cap droplet PS-PMMA(27.0 k), and (b) an ordered hyperbolic droplet PS-PMMA(55.6 k).

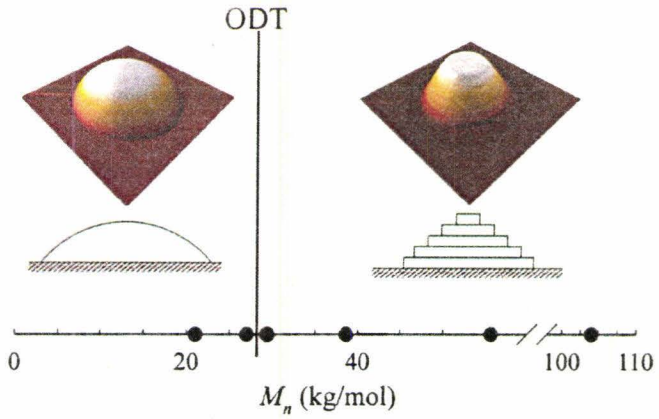

FIG. 4 (color). Phase diagram of the droplet order as a function of the total molecular weight at a temperature of 180 °C.

out for droplets with M_n ranging from 21 kg/mol to 104 kg/mol (see Table I). Using the discriminant to distinguish between the ordered and disordered droplets we obtain the results shown in Fig. 4. In changing the total M_n of the symmetric diblock from 27.0 kg/mol to 29.4 kg/mol, the system passes from being disordered to being ordered, which is consistent with the bulk ODT observed at $M_n \approx 28$ kg/mol [31].

Here we have shown that an anisotropic liquidlike a diblock copolymer can form droplets which deviate from the classical spherical cap. An ordered droplet will orient its lamellae along the substrate because of a preferential interaction between the substrate and one of the blocks. There are two competing interactions which lead to the hyperbolic profile: (1) the edge tension which drives material from a higher (smaller) disk into a lower (larger) disk—analogous to a small soap bubble in contact with a large bubble and (2) the edge repulsion which prevents two adjacent edges from coming too close to each other. The process of smaller disks emptying into larger disks continues, with very slow kinetics compared to defining the hyperbolic shape, making an equilibrium treatment reasonable. An extreme example of this is shown in Fig. 5. In this final stage of the morphology only one bilayer disk remains on a monolayer surface which undergoes a fingering instability as it spreads onto the substrate.

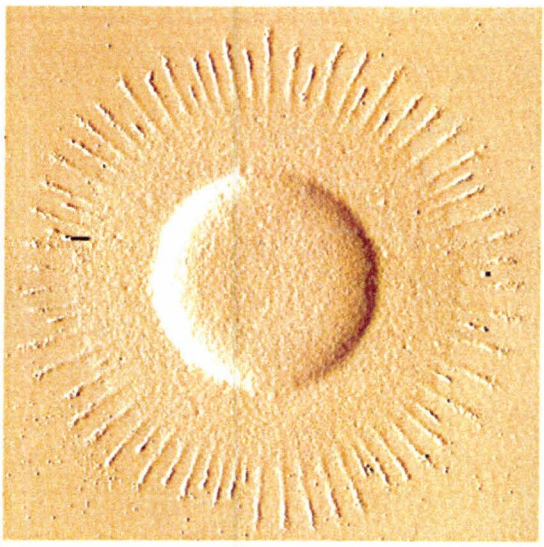

FIG. 5 (color). Error signal of a "droplet" consisting of a single bilayer disk. The 20×20 μm AFM scan of a diblock droplet PS-PMMA(29.4 k) shows a single bilayer disk on a monolayer carpet. There is a well-defined periodic fingering instability associated with the spreading monolayer.

The authors thank Günter Reiter and An-Chang Shi for valuable discussions. Financial support from NSERC, PREA, CFI, and OIT of Canada are gratefully acknowledged.

*Electronic address: dalnoki@mcmaster.ca

[1] P. G. de Gennes, F. Brochard-Wyart, and D. Quéré, *Capillarity and Wetting Phenomena* (Springer-Verlag, Berlin, 2004).
[2] R. Blossey, Nat. Mater. **2**, 301 (2003).
[3] A. Otten and S. Herminghaus, Langmuir **20**, 2405 (2004).
[4] J. Bechhoefer and P. Oswald, Europhys. Lett. **15**, 521 (1991).
[5] H. Gau *et al.*, Science **283**, 46 (1999).
[6] F. S. Bates and G. H. Fredrickson, Phys. Today **52**, No. 2, 32 (1999).
[7] M. W. Matsen, J. Phys. Condens. Matter **14**, R21 (2002).
[8] M. J. Fasolka and A. M. Mayes, Annu. Rev. Mater. Res. **31**, 323 (2001).
[9] G. H. Fredrickson, Macromolecules **20**, 2535 (1987).
[10] B. L. Carvalho and E. L. Thomas, Phys. Rev. Lett. **73**, 3321 (1994).
[11] K. Binder *et al.*, J. Phys. II **7**, 1353 (1997).
[12] R. Limary and P. F. Green, Langmuir **15**, 5617 (1999).
[13] P. Busch *et al.*, Macromolecules **36**, 8717 (2003).
[14] D. Ausserre *et al.*, J. Phys. II **3**, 1485 (1993).
[15] M. S. Turner *et al.*, J. Phys. I **5**, 917 (1995).
[16] P. F. Green and R. Limary, Adv. Colloid Interface Sci. **94**, 53 (2001).
[17] R. Limary *et al.*, Eur. Phys. J. E **8**, 103 (2002).
[18] P. Müller-Buschbaum *et al.*, Macromolecules **35**, 2017 (2002).
[19] I. Podariu and A. Chakrabarti, J. Chem. Phys. **118**, 11 249 (2003).
[20] P. F. Green, J. Polym. Sci., Part B: Polym. Phys. **41**, 2219 (2003).
[21] S. H. Kim *et al.*, Adv. Mater. **16**, 2119 (2004).
[22] R. A. Segalman *et al.*, Phys. Rev. Lett. **91**, 196101 (2003).
[23] E. Huang *et al.*, Nature (London) **395**, 757 (1998).
[24] T. Thurn-Albrecht *et al.*, Adv. Mater. **12**, 787 (2000).
[25] F. Heslot *et al.*, Nature (London) **338**, 640 (1989).
[26] S. Betelú *et al.*, Phys. Rev. E **59**, 6699 (1999).
[27] J. de Coninck *et al.*, Phys. Rev. Lett. **74**, 928 (1995).
[28] M. P. Valignat *et al.*, Phys. Rev. Lett. **77**, 1994 (1996).
[29] R. Lucht and Ch. Bahr, Phys. Rev. Lett. **85**, 4080 (2000).
[30] P. Oswald and L. Lejček, Eur. Phys. J. E **19**, 441 (2006).
[31] T. P. Russell, R. P. Hjelm, and P. A. Seeger, Macromolecules **23**, 890 (1990).

EPJ manuscript No.
(will be inserted by the editor)

Spreading of diblock copolymer droplets: a probe of polymer micro-rheology

Andrew B. Croll[1] and Kari Dalnoki-Veress[1] [a]

Department of Physics & Astronomy and the Brockhouse Institute for Materials Research, McMaster University, Hamilton, ON, Canada.

March 3, 2009

Abstract. We present an experimental study of the spreading dynamics of symmetric diblock copolymer droplets above and below the order disorder transition. Disordered diblock droplets are found to spread as a homopolymer and follow Tanner's law (the radius grows as $R \sim t^m$; where t is time and $m = 1/10$). However, droplets that are in the ordered phase, are found to be frustrated by the imposed lamellar microstructure. This frustration is likely at the root of the observed deviation from Tanner's Law: droplet spreading has a much slower power law ($m \sim 0.05 \pm 0.01$). We show that the different spreading dynamics can be reconciled with conventional theory if a strain-rate dependent viscosity is taken into account.

PACS. 83.80.Uv Block copolymers – 68.08.Bc Wetting – 82.35.Gh Polymers on surfaces; adhesion – 47.55.Dz Drops and bubbles

1 Introduction

The spreading of liquid droplets on solid substrates has long facinated many researchers [1–8]. A firm understanding of the details governing droplet dynamics is crucial for many industrial processes and serves as a testing-ground for the physics of capillarity [1]. The wetting of a surface by droplets of simple fluids [2–4], as well as more complex polymeric fluids [5–8] has therefore received much attention.

Tanner, who studied the spreading of poly(dimethylsiloxane) droplets, noted that the apparent contact line of the droplets spread in time with the characteristic power law of t^m; where $m = 1/10$ – commonly referred to as Tanner's law [2]. Tanner also discussed the complexities of a hydrodynamic solution due to divergences in the vicinity of the contact line, which is related to a nanoscopic precursor film that spreads diffusively ahead of the contact line of the droplet. The existence of the precursor film was suggested by the earlier experiments of Hardy [9], and this film was found to cover the substrate quickly compared to the spreading of the bulk droplet. As a result the macroscopic wetting that is observed is a consequence of the bulk droplet spreading on a microscopic film of the same material, thus removing the chemical details of the surface from the problem.

The dynamics of wetting was put on firm theoretical footing by de Gennes who developed a hydrodynamic theory which correctly predicted the scaling relationship

$$R(t) \sim \left(\frac{\gamma}{\eta}\right)^{\frac{1}{10}} \Omega^{\frac{3}{10}} t^{\frac{1}{10}}; \qquad (1)$$

where R is the position of the apparent contact line, γ is the surface tension, η is the viscosity, and Ω is the droplet volume [10]. In this formalism, the energy gained by spreading is balanced by the energy lost to viscous dissipation in a wedge of fluid near the apparent contact line of the drop. The universality of the wetting dynamics was shown by de Gennes to be due to the presence of the precursor layer. As a result of this layer, the droplet spreads with a power-law that is independent of the substrate. Since the energy gained by covering the substrate surface is dissipated in the precursor film alone, the droplet dynamics is entirely due to the Laplace pressure reducing the curvature of the droplet as it spreads on the precursor.

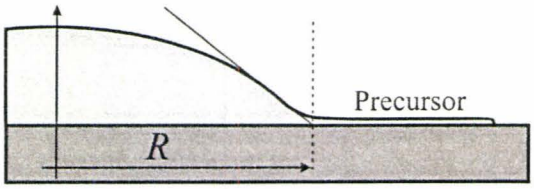

Fig. 1. The geometry of a spreading droplet with radius, R, volume, Ω, surface tension, γ, and viscosity, η. Also illustrated is a precursor wetting layer which spreads ahead of the bulk droplet.

[a] email: dalnoki@mcmaster.ca

Diblock copolymers, molecules made of two chemically distinct polymer blocks with monomers 'a' and 'b' covalently bonded to one-another, are widely studied and find increased use as a compatibilizing agent between two surfaces (for example as a coating on an unfavorable substrate) due to their amphiphilic nature [11–13]. Because of the chemical incompatibility of polymer blocks a and b, diblock copolymers are found to phase separate as they pass through the order disorder transition (ODT). The connectivity of the blocks limits the length scale of the phase separated domains to that of the molecular size (~10 nm). The geometry of the morphology depends on the natural curvature induced by the ratio of the two block lengths and the stretching of the chains required to accommodate the morphologies with long-range periodic order. Here we deal with the simplest case: a symmetric diblock where the a and b components are of equal size favouring the zero curvature microstructure of lamellae [12,14]. The phase transition as the system passes through ODT is most easily understood through changes in the temperature, T: high temperature favours the entropy of the polymer coils as they randomly fill space, whereas at low temperature the enthalpy dominates which drives the segregation of the blocks to minimize a and b contacts. Though somewhat less intuitive, ODT can also be traversed through changes in molecular weight. In this case increasing the molecular weight, M_N, leads to increasing the enthalpic contribution and hence ordering; this is because the energy cost of removing a block from its preferred domain is proportional to its size. Thus, the ordered state can be obtained by increasing the molecular weight of the molecules or by decreasing T. These two effects are generally combined as χN, where N is the number of segments in a chain, and χ is the Flory-Huggins interaction parameter (typically written as $\chi = A/T + B$).

The microstructure of a block copolymer melt significantly changes its rheology [11,15]. When in a disordered state a diblock copolymer responds much like a homopolymer and the timescales of flow are set by the length of the polymer. When microphase separation takes place, the structure imposed on the fluid adds complexity to its rheological response (for example, see figure 6 of [11]). One might expect the addition of structure to result in an additional barrier to flow, which naturally raises several questions: Does the underlying structure affect droplet spreading in an observable way? Can the flow of diblock copolymer droplets be understood in the same manner as that of more simple fluids? Here we address these questions with an experimental study of the spreading of symmetric diblock copolymer droplets. We find that the droplet spreading is comparable to simple polymeric fluids when the polymer is in the disordered state, while the flow during spreading is significantly impeded in the ordered state. The slow dynamics observed here can be understood when the spreading dynamics theory of de Gennes is coupled with a viscosity that is dependent on the microstructure.

Table 1. Polymer Details: the number averaged molecular weights for the PS and PMMA blocks, the polydispersity index, and the microstructural state at 180°C (D-Disordered, O-ordered) [16].

M_N^{PS} (kg/mol)	M_N^{PMMA} (kg/mol)	PI	Phase
10.0	10.0	1.05	D
12.8	12.9	1.05	D
14.9	13.1	1.05	O
18.0	18.0	1.07	O
25.0	26.0	1.09	O
52.0	52.0	1.09	O

2 Experiment

Electronics grade Si substrates (University Wafer, USA) with the native oxide layer present were cleaned with super critical CO_2 ('Snow jet', Applied Surface Technologies, USA) and UV-ozone treatment, which will largely eliminate surface contamination. The resulting substrates were completely wetted by the polymers used in this study: a series of symmetric monodisperse poly(styrene-methyl methacrylate) (PS-PMMA) of various total M_N, obtained from Polymer Source (Dorval, Quebec). Details of the polymers used in this study can be seen in Table 1. We note that when we discuss the molecular weight of a system we refer to the total weight of the molecule, with each block composing half the total mass. There is a slightly lower interfacial tension between PMMA and the substrate than that of PS and the substrate. Furthermore, PS has a lower surface tension than does PMMA at the temperatures studied. As a result, when ordered, the wetting precursor layer on the substrate is a monolayer allowing PMMA contact with the substrate and PS with air. All additional layers will be bilayers in order to maintain a PS-air interface i.e. Si/PMMA-PS/PS-PMMA PMMA-PS/etc.

The PS-PMMA was 'dusted' onto a substrate, heated, and observed via optical microscopy. Several molecular weights were used, ranging from molecules with 20 kg/mol to 104 kg/mol. From previous work it was known if the droplets were in the ordered or disordered state (see table 1 for the details) [16]. All experiments were carried out on a microscope hot stage (Linkam Scientific, UK) at 180°C as well as in a separate home-built vacuum oven. Some substrates were spin-coated with a monolayer of diblock from a dilute polymer solution in toluene prior to use. Since a monolayer precursor film is expected to form ahead of the spreading droplet, comparison of droplet spreading on either substrate should be equivalent. There was no difference between the spreading dynamics of experiments on the Si substrate or those pre-coated with a monolayer. The test on the two substrates shows unambiguously that there is a precursor layer in front of the bulk droplet and that the final state is a totally wet substrate.

Droplet radii were measured with reflection optical microscopy. White light was filtered with a green notch

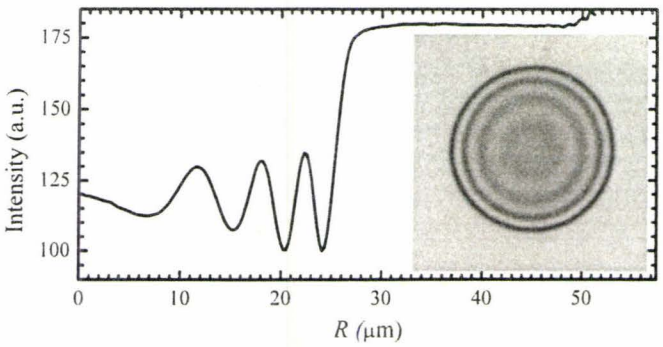

Fig. 2. An average intensity profile from a typical droplet (shown in inset). In this case the droplet is made up of a 20 kg/mol disordered diblock copolymer.

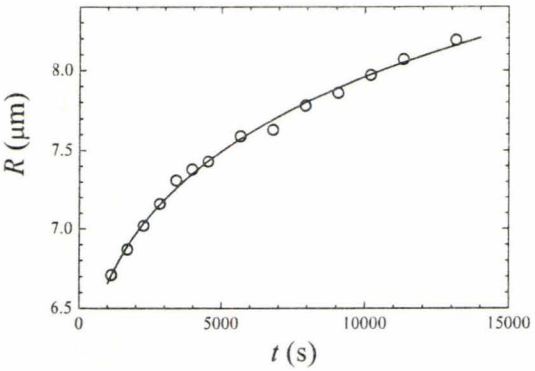

Fig. 3. Radius as a function of time for the spreading of a typical disordered diblock copolymer droplet. Shown is data from a 20 kg/mol droplet on a Si substrate. The curve is a power law fit with exponent 0.096 ± 0.004.

filter (centered at 533 nm, FWHM 10 nm) in order to improve our measurements which depend on interference fringes. Software was developed which located a droplet center and then averaged the interference fringes of the droplet around this point (see figure 2). The fringes were converted into topography data and fit with the generic equation $0 = Ax^2 + Bxy + Cy^2 + Dx + Ey + F$. Fitting to this droplet profile was used because we have previously found that ordered droplets can have a hyperbolic profile; thus this simple form is valid in the case of hyperbolic or spherical cap droplets and can be used to determine the state of order [16]. The fit function was extrapolated to the substrate to yield the dynamic contact angle, θ_D, and radius of the contact line, R. Since the bulk droplet 'leaks' into the precursor layer, by accessing both θ_D and R, the droplet volume could be monitored thereby ensuring that the volume of the droplet was constant as required in the theory. The use of the interference fringes limits the droplets included in this study to those such that the fringes nearest the edge could still be easily resolved (contact angles $< 30°$).

Atomic force microscopy (AFM) was used in order to independently verify the microstructure of the droplets and contact angle (Caliber, Veeco, USA). These measurements involved quenching samples to room temperature, well below the glass transition, and then scanning with tapping mode with AFM. No significant deviations from the optical experiments were found.

3 Results and discussion

3.1 Disordered droplets

A typical spreading curve for a disordered diblock copolymer can be seen in figure 3. The solid line is a fit to the power law $R(t) \sim (t - t_0)^m$, where m and t_0 are fitting constants. The time offset is crucial because the start of flow is not clearly defined both because the drop does not start as a perfect spherical cap and because the time at which flow begins is not exactly when the accumulation of images starts. The radius is found to grow as a power law in time with an exponent of 0.096 ± 0.004 – a scaling that is consistent with the spreading of simple fluids and homopolymers in accordance with Tanner's law. This scaling was typical of all droplets studied in the disordered regime ($M_N = 20$ and 26 kg/mol).

The rheology of homopolymers is well known to be non-linear, particularly if the polymer length is above the entanglement length, where the polymer diffusion becomes significantly slowed by the topological constraints imposed by other chains [18]. In general the polymer viscosity will depend on the shear strain rate and shear thinning is observed beyond some critical shear strain rate. Here we simply estimate the shear strain rate as the spreading velocity divided by the droplet height, H. For the droplet in fig. 3, using the largest velocity, $V/H \sim (0.3 \text{ nm/s})/(800 \text{ nm})$, we estimate shear rate to be below $\sim 10^{-4}$ s^{-1} over the course of the experiment. Comparison to work by other researchers reveals that this is well below the critical shear strain rate, validating the constant value of the viscosity used in the derivation of Tanner's law and the results obtained in the experiments described here (see figure 1 of reference [15] which shows that this system is well within the terminal flow region). With a constant viscosity there is no significant difference in the spreading dynamics between disordered block copolymers and simple fluids, and therefore we can easily understand the good agreement with the predicted 1/10 power law.

3.2 Ordered droplets

Figure 4 shows the radius as a function of time for several droplets of 36 kg/mol molecules. This system is ordered at 180°C [16]. These droplets flow in a different manner. Initially, spreading is in agreement with Tanner's law – a power law exponent of $\sim 1/10$. However after some time (~ 5000 s) flow crosses over to follow a power law with a lower exponent. This slower spreading has been observed for all the molecular weights studied in the ordered regime (see table 1), on both the Si and monolayer covered substrates, in air and under vacuum. The slower spreading region is well fit by an exponent of 0.05 ± 0.01: we stress that the power law scaling is still consistent with the data,

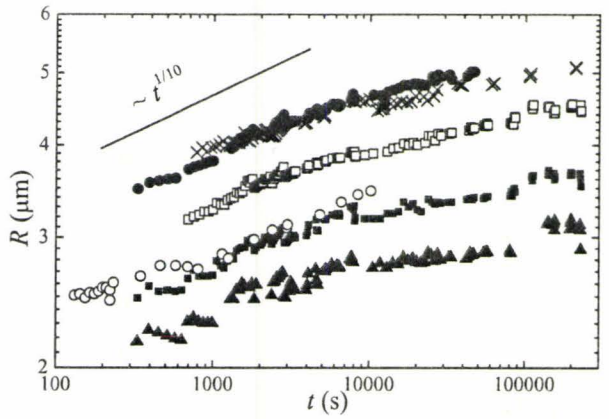

Fig. 4. A double logarithmic plot of the contact radius of several 36 kg/mol diblock copolymer drops of differing volume as a function of time at 180°C. At these temperatures, this system is in the ordered lamellar regime. The observed noise on the signal is related to focal drift over the course of the experiment.

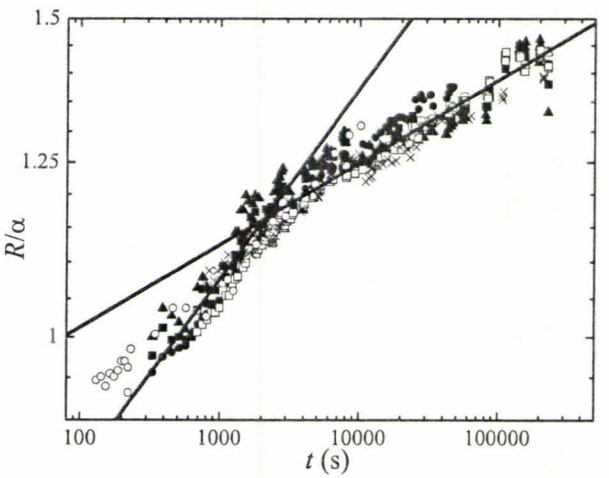

Fig. 5. Data from figure 4 scaled by dividing by a scaling parameter, α, described in the text. Note that this one parameter is enough for the data to collapse on the same curve.

but with a smaller exponent than the expected 1/10 value of Tanner's law.

In figure 5 we rescale the data of of figure 4 by normalizing the data by a prefactor, α. The normalization is chosen such that the data sets collapse and correspond to unity at 500 s. Comparison with Tanner's law (eq. 1) reveals that the prefactor is dependent on viscosity, surface tension, and the volume of the drop, $\alpha \sim (\gamma/\eta)^{1/10}\Omega^{3/10}$. Since η and γ are the same for the set of 36 kg/mol droplets shown in figure 5, we plot the scaling parameter as a function of the volume of the droplets in figure 6. This is well fit by a power law with an exponent of 0.29 ± 0.03, consistent with that predicted by Tanner's law.

We suggest that the basis of the crossover from Tanner's law to a different power law is the result of increasing ordering in the droplets. In the initial stages of growth the droplets are not well ordered, both because ordering takes

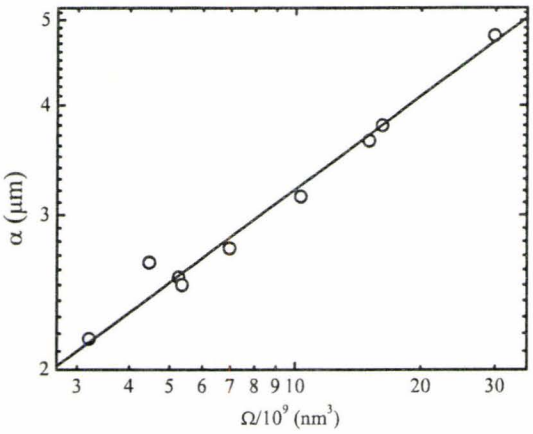

Fig. 6. In this figure we show a log-log plot of the scaling parameter as a function of volume for the 36 kg/mol droplets. The line is a power law fit with a slope of 0.29 ± 0.03.

time and because the growth rate is most rapid initially which may impede ordering. The initial spreading dynamics is analogous to disordered droplets and hence follows Tanner's law. However, as the spreading proceeds, the velocity decreases and eventually larger lengthscale lamella parallel to the substrate start to dominate [16]. Once significant order appears flow is frustrated further, i.e. more complex rearrangement of lamellae and polymer molecules in one layer have to overcome a hopping barrier to flow into an other layer [23]. The ordering results in a change in the rheology of the fluid in the droplet – as the droplet velocity slows, order increases, and the effective viscosity increases. This is similar to the increasing viscosity with decreasing frequency of rheological experiments which has been observed in block copolymer samples, see for example [15]. We can estimate the shear strain rate from the data in figure 4 and the droplet size to be $\sim 10^{-3}$ s^{-1} at the cross-over from fast to slow behavior. This is approximately where the modulus of a block copolymer is known to show power law behavior [15], which suggests that one might expect a non-linear viscosity in the spreading droplet.

Based on the observation that the flow is impeded, we make the following simple assumption: the viscosity varies inversely with the shear strain rate as $\eta \sim \eta'\dot{\varepsilon}^{-\beta} \sim \eta'(h/V)^{\beta}$; where β is a positive constant, h is the height of the droplet wedge at some point near the contact line, and V is the average velocity of the contact line. We note that this is similar to what is expected for shear thinning fluids and follow the theory presented by Rafaï and coworkers on that topic [24], which we describe briefly here. We take as starting point that the energy that drives the spreading is balanced by the energy dissipated in the fluid wedge at the contact line (see [1,10]),

$$\frac{\gamma\theta_D^2 V}{2} = \int_a^R \int_0^h \eta \left(\frac{dV}{dz}\right)^2 dz\, dx; \qquad (2)$$

where the driving force comes from the surface tension, γ, and the contact angle, θ_D. The integrals are over the

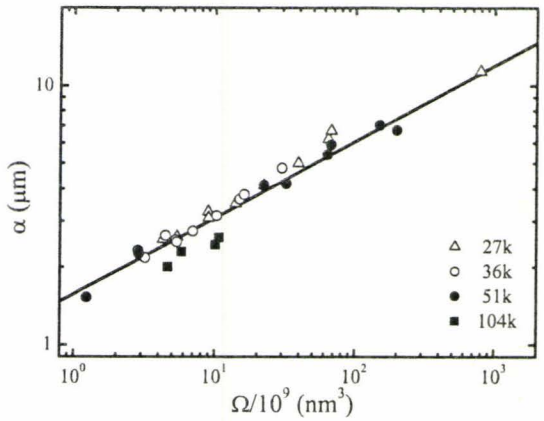

Fig. 7. A log-log plot of the scaling factor α (see text) obtained in the creation of master plots for various molecular weights, as a function of volume. The solid line is a best fit to the data excluding the 104 kg/mol sample $\alpha \sim \Omega^{0.29\pm0.03}$

height of the droplet and the radial distance; the details of the small lengthscale cutoff, a, depends on the molecular scale and is well discussed in [1,10]. Assuming Poiseuille flow, that θ_D is small, and near the wedge $h \sim \theta x$, one obtains

$$R \sim \left(\frac{\gamma}{\eta'}\right)^{\frac{1}{10-3\beta}} \Omega^{\frac{3-\beta}{10-3\beta}} t^{\frac{1-\beta}{10-3\beta}}; \qquad (3)$$

which is in full agreement with the expression obtained by Rafaï and coworkers for shear thinning. Equation 3 represents a modified Tanner's law which includes the possibility of a non-linear viscoelasticity that can be described by $\eta \sim \eta'\dot{\varepsilon}^{-\beta}$. The best fit to the slow growth regime shows $R \sim t^m$ with $m = 0.05 \pm 0.01$. Since $\beta = (1-10m)/(1-3m)$, the non-linear viscosity seen in the spreading experiments corresponds to $\eta \sim \eta'\dot{\varepsilon}^{-(0.59\pm0.14)}$. We can compare this result with those obtained previously on bulk samples and find that the droplet spreading non-linear viscosity is consistent with rheological experiments on diblock copolymers which result in $\beta \sim 0.5$ [15]. We note that this exponent is different from what would be expected for the shear thinning of a simple homopolymer, $\eta \sim \eta'\dot{\varepsilon}^{-1}$ [18].

3.3 Molecular Weight Effects

We now turn to the effect of molecular weight on the droplet spreading. In order to determine if any molecular weight effects existed in this system, the same master plots as described above were constructed for all ordered samples (see table 1). The scaling parameters were then plotted as a function of volume as can be seen in figure 7. For all molecular weights except perhaps the 104 kg/mol sample, the data falls along the same power law. Since a vertical shift in these data is related to surface tension and viscosity as seen in equation 3, the fact that all the data lies on the same general curve may initially seem counterintuitive as homopolymer viscosity is highly molecular weight dependent. However, in a partially ordered sample the molecular domains are segregated and spreading takes place mainly through lamella sliding past one-another, and the rheology is primarily a result of this microstructure [17]. The viscous losses are therefore determined by the molecular friction of the lamella sliding an effect that is amplified by shearing [19]. With a small interpenetration or entanglement between lamellae, there is no longer any physical reason for molecular weight to contribute as significantly to the flow as for an entangled polymer melt. The highest molecular weight polymer used in this study, 104 kg/mol, does show some small deviation from the general trend, indicating that the greater penetration of chains into adjacent lamellae expected for higher molecular weights, may be starting to become important.

4 Conclusions

We have observed a significantly impeaded flow in ordered diblock copolymer droplets. Droplets that consist of a diblock molecular weight that is disordered show spreading dynamics consistent with Tanner's law. However upon increasing the molecular weight and passing into the ordered regime, the droplets initially follow Tanner's law and then proceed with a slower dynamics. We show that the late stage spreading is consistent with a modified spreading law that takes into account the non-linear viscoelastic effects of the ordered diblock copolymer melt. The picture that emerges is one where as the degree of order increases, both because more time has elapsed and because the flow proceeds more slowly, the droplets crossover from a faster to a slower growth dynamics. The slowing is then related to the frustration induced by the lamellar microstructure of the droplets. We show that that this effect persists through many ordered molecular weights. Our experiments show no dependence of the spreading on the molecular weight of the diblock when ordered with a possible exception of the highest molecular weight studied. This suggests, in agreement with other studies, that the character of this fluid is primarily a result of the lamellar structure, and the sliding of lamellae, not of the polymeric nature of the material.

Financial support from NSERC and the ACS PRF are gratefully acknowledged.

References

1. P.G. de Gennes, F. Brochard-Wyart, and D. Quéré, *Capillarity and Wetting Phenomena.* (Springer-Verlag New York Inc., 2002) 139-151.
2. L.H. Tanner, J. Phys. D: Appl. Phys. **12**, 1473 (1979).
3. M.D. Lelah and A. Marmur, J. Colloid Interface Sci. **82**, 518 (1981).
4. G. He, and N.G. Hadjiconstantinou, J. Fluid. Mech. **497**, 123 (2003).

5. D. Ausserré, A.M. Picard, and L. Léger, Phys. Rev. Lett. **57**, 2671 (1986).
6. L. Léger, M. Erman, A.M. Guinet-Picard, D. Ausserré, and C. Strazielle, Phys. Rev. Lett. **60**, 2671 (1988).
7. E. Pérez, E. Schäffer and U. Steiner, J. Colloid Interface Sci. **234**, 178 (2001).
8. D.R. Heine, G.S. Grest, and E.B. Webb III, Phys. Rev. E **68**, 061603 (2003).
9. W. Hardy, Philos. Mag. **38** 49 (1919).
10. P.G. de Gennes, Rev. Mod. Phys. **57**, 827 (1985).
11. G.H. Fredrickson, and F.S. Bates, Annu. Rev. Mater. Sci. **26**, 501 (1996).
12. M.J. Fasolka, and A.M. Mayes, Annu. Rev. Mater. Sci. **31**, 323 (2001).
13. F.S. Bates, and G.H. Fredrickson, Annu. Rev. Phys. Chem. **41**, 525 (1996).
14. Matsen, M. W., J. Phys.: Condens. Matter, **14**, R21 (2002).
15. H. Braun, W. Gleinser, and H.-j. Cantow, J. Appl. Poly. Sci. **49**, 487 (1993).
16. A. B. Croll, M. V. Massa, M. W. Matsen, and K. Dalnoki-Veress, Phys. Rev. Lett. **97**, 204502 (2006).
17. R.G. Larson, K.I. Winey, S.S. Patel, H. Watanabe, and R. Bruinsma, Rheol. Acta. **32**, 245 (1993).
18. W.W. Graessley, Adv. Poly. Sci. **16**, 1 (1974).
19. T.A. Witten, L. Leibler, and P.A. Pincus, macromolecules. **23**, 824 (1990).
20. C. Poulard, and A.M. Cazabat, Langmuir **21**, 6270 (2005).
21. P.G. de Gennes, and J. Prost, *The Physics of Liquid Crystals.* (Oxford University Press, Toronto, 1993) 198-220.
22. J. L. Ericksen, Trans. Soc. Rheo. **13**, 9 (1969).
23. A.B. Croll, M.W. Matsen, A.-C. Shi, and K. Dalnoki-Veress, Eur. Phys. J. E, (2008).
24. S. Rafaï, D. Bonn, and A. Boudaoud, J. Fluid. Mech., **513**, 77 (2004).

Fingering Instability of a Spreading Lamella

Andrew B. Croll and Kari Dalnoki-Veress
*Department of Physics & Astronomy and the Brockhouse Institute for Materials Research, McMaster University, Hamilton, ON, Canada**
(Dated: December 18, 2008)

An atomically thin wetting layer quickly spreads from the base of a droplet of fluid placed on a favourable substrate. In a lamella forming fluid this presents a problem, the film's lowest free energy state is one of lamellar thickness, which a film cannot maintain far from the fluid reservoir. The result of this frustration is an intricate pattern of equally spaced dendritic fingers, which we investigate in this letter. Atomic Force Microscopy (AFM) measurements reveal a morphological progression from densely spaced dendritic fingers to cellular patterns as small to large droplets are observed. As the morphology strongly suggest an analogy to the solidification of metal crystals in the presence of a solute, we proceed to analyze our findings in terms of the Mullins-Sekerka instability. Using the strong segregation limit to describe the wetting monolayer, we find fair scaling agreement with the predictions of the standard linear stability analysis. We finish our discussion by presenting the molecular weight dependence of the onset of the instability.

PACS numbers: 61.25.Hq

The study of soft condensed matter systems is riddled with examples of intricate self-assembled mesoscopic patterns [1–8]. The 'fingering' instability is an example of a simple type of pattern wherein a material forms regularly spaced intrusions from one phase into another. These non-equilibrium intrusions are ubiquitous in nature, forming for a number of different reasons in many different systems. However, fingering only occurs when there is a competition between two different interfacial conditions. An excellent example is the 'tears' that occur in a thin film of wine on the side of a glass. Due to the surface tension gradient formed by the evaporating alcohol the film is driven up the glass and a competition arises between the energetic cost of newly created interface and the viscous dissipation incurred in moving the wine to accommodate the new shape [2]. The viscosity favours small features (less distance to move the fluid) whereas the interfacial energy favours larger features (less surface area). The solution is the fastest growth of an intermediate scale fluctuation (often on the order of microns in soft matter systems). A particularly striking, and previously unstudied example of a fingering instability is evident in the spreading of block copolymer droplets on silicon substrates (see Fig. 1). In this letter we experimentally investigate this spontaneous pattern formation and show that it falls into the universality class of the ubiquitous Mullin-Sekerka instability.

Diblock copolymers are extended molecules made by joining a sequence of monomers of one variety (A, for example), to a sequence of some other type of monomer (in this case B). A melt of diblock molecules is well known to spontaneously form a rich variety of internally ordered states when below an Order to Disorder Transition (ODT) temperature, due to the chemical dissimilarity of A and B. While many geometries (spheres, cylinders, lamella) can be formed as the ratio of sequence lengths deviates from 1/2, here we will only consider

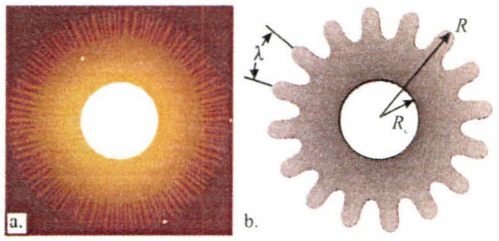

FIG. 1: a. a typical droplet in which the lamellar wetting front has become unstable. b. a schematic of the geometry used throughout to characterize the pattern.

the lamellar state formed by symmetric molecules. This choice is made primarily for simplicity, but secondly because all but the most extreme, asymmetric molecules will form a lamellar wetting layer on a substrate that is highly attractive to one block. We ensure the substrate is completely wet by the diblock simply by choosing a molecule/substrate combination that has just this property.

In a typical experiment, a silicon substrate (University Wafer) is cleaned by super-critical CO_2 and then by 40 minutes of UV-ozone treatment. This results in a highly reliable substrate for these experiments. We stress that the substrate preparation is critical for the instability to appear as we show here, due to the strong dependence of wetting phenomena on the fine details of the surface energy. After UV-Ozone treatment, samples are immediately "dusted" with freeze-dried diblock copolymer (Polymer Source, inc.) and placed on a hot stage (Linkam Scientific) under argon flow. Samples can then be quenched into their glassy room temperature state after annealing for some pre-determined time and explored with an atomic force microscope (AFM). We use a Veeco Caliber in tapping mode for the studies described here.

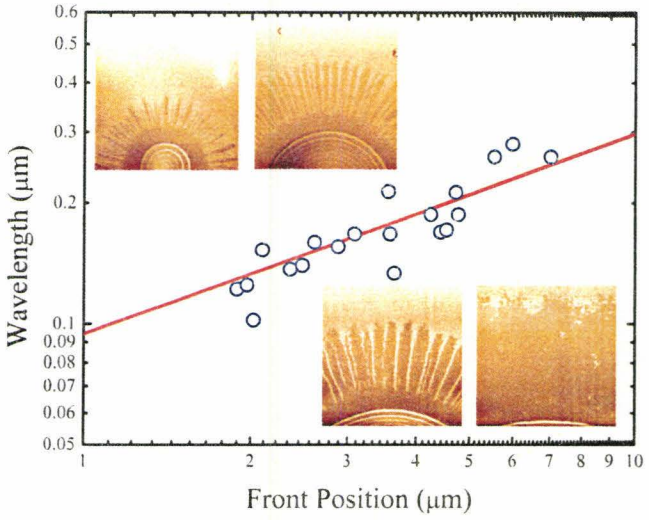

FIG. 2: Log-log plot of the instability wavelength as a function of front position for several droplets of the 36 kg/mol samples. The insets show $10 \times 10\mu$m AFM phase images of several droplets, illustrating the morphological progression as the front position becomes larger. The solid line is a fit to the function $a\sqrt{R}$, where $a = 0.094\ \mu\text{m}^{1/2}$.

Fig. 2 shows the wavelength of the instability as a function of front position for several droplets of $N = 353$ symmetric copolymer. The insets of this figure show AFM phase images of the morphological progression of the instability. Small droplets have fingers that are more dendritic in character, and as the distance to the front gets larger the pattern becomes progressively more cellular. This morphological progression qualitatively suggests an interpretation in analogy with a solidifying binary mixture, as many studies of solidifying alloys show the cellular to dendritic transition taking place as front velocity increases [9]. We note the wavelength also noticeably increases with the distance to the front position.

Superficially the spreading diblock copolymer film seems quite similar to the wine glass example. As in any fluid wetting a substrate, a thin film spreads away from the droplet to minimize the surface energy [10]. This microscopic layer is not unstable in the same manner as is the wine, because there is no significant thickness to the moving fluid (hence gravity can safely be ignored). An extremely thin polymer film slides across the substrate, in contrast with the Poiseuille flow of a much thicker film [11]. The anisotropic nature of the diblock copolymer molecules causes there to be an additional energetic penalty to this flow as the molecules would prefer to remain separated into A rich or B rich lamellar domains. This order, which prefers a fixed lamellar thickness, must compete with the natural tendency of a fluid film spreading from a source to thin as its front progressively covers more area. It is this additional frustration that leads to a destabilizing effect, not on the wetting front, but some distance away where the areal density of polymer is high enough to form a lamellar layer.

The two necessary physical effects for a fingering instability are present, a viscosity (or sliding friction) that makes long wavelengths unfavorable and an edge tension that makes small features costly. The instability arises because there is a difference in chemical potential between a molecule in the lamella and a molecule in the surface wetting phase. This difference causes liberation of some small amount of energy at the interface which must also be dissipated away. This places this effect in the category of the Mullins-Sekerka (MS) instability, the same instability that describes the formation of dendritic fingers in solidifying alloys, snowflakes, and many other systems [12, 13].

Mullins and Sekerka first derived the criteria for the stability of front propagation in a two component system [12]. In our case the two components correspond to ordered diblock copolymer in a lamella, and the disordered diblock copolymer that can no longer form a lamella. The interphase between these two states moves with velocity v away from the center of the droplet. The wavelength is then given simply by $\lambda \sim \sqrt{l\kappa^{-1}}$. l is a diffusion length, and can be rewritten as $2D/v$ with D a diffusion constant. κ^{-1}, the capillary length, is best defined through a chemical model of the interface as $\Gamma/(\Delta C)^2(\partial\mu/\partial C)$; where Γ is an edge tension, C is the areal concentration, ΔC the areal concentration gap, and μ is the chemical potential (see [13] for a more detailed discussion of the chemical model). The edge tension in this system will mainly be due to the new surface created at the interphase and can be written $\Gamma \sim \gamma L$ where γ is simply the surface tension of polystyrene (which is always situated on the air interface) and L is the lamellar thickness. In this form, however, the wavelength prediction is somewhat unruly due to the dependence on velocity (which results from the balance of forces acting on the fluid) and the details of the chemical potential.

The flow in a thin film has been thoroughly investigated in polymeric systems [14–17]. It is most simply understood by comparison of the frictional energy dissipated by the film sliding over the substrate and the energetic gain of the film covering the surface. From a scaling point of view, the friction can be characterized as $\xi v\pi R^2$, where ξ is a constant describing the magnitude of the friction, v is velocity and πR^2 is the amount of fluid in contact with the substrate (R is the position of the front). The surface energy is described by the spreading parameter S in combination with the amount of front ($2\pi R$) present. Balancing the two gives the front position as $R \sim \sqrt{St/\xi}$, where t is the time. This is the same form as one might expect from a diffusion argument if the diffusion constant is replaced as $D = S/\xi$. The diffusion constant has been thoroughly characterized by others [16, 17]. The velocity can then be directly related to the position of the front ($R \sim \sqrt{Dt}$ so

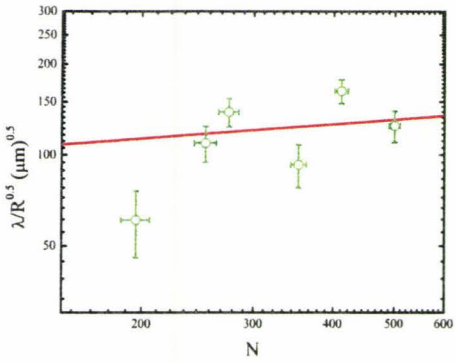

FIG. 3: The instability wavelength (scaled by $\sqrt{R}$) is shown as a function of N. The Solid line is a fit to the function $aN^{1/6}$ where $a = 48\mu\text{m}^{0.5}$.

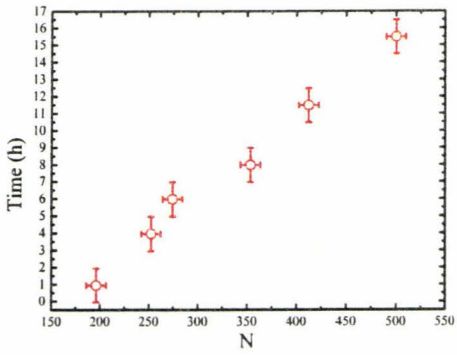

FIG. 4: A diagram illustrating the regions of instability (open symbols and vertical bars) and stability (everywhere else) for several molecular weights. A clear linear relationship between the critical time and N is shown

$v \sim \sqrt{D/t} \sim D/R$).

In order to calculate the areal concentration we begin with the assumption that the block copolymer in its ordered state can be described by the strong segregation limit. While strictly speaking this assumption is not true in the bulk for the molecular weights considered here, its analytic nature and success in describing the main physical ideas behind microphase separation make it attractive. Furthermore, because of the high affinity of one of the blocks for the substrate, the strong-stretching theory should provide an adequate perspective. In this framework the lamellar thickness scales as $L \sim a\chi^{1/6}N^{2/3}$ [18, 19]. The areal concentration in the brush can then easily be calculated as $C_{brush} \sim a^{-2}\chi^{1/6}N^{-1/3}$. Likewise the disordered concentration is $C_{flopped} \sim a^{-2}N^{-1}$. Therefore the change in concentration at the front is $\Delta C \sim C_{brush}$, as one might expect. The chemical potential can also be calculated from the strong segregation free energy which allows the simple calculation of $\partial\mu/\partial C$, which we find to be $\sim (\chi N)^{1/3}$. The wavelength is therefore given by the much more experimentally accessible form

$$\lambda \sim \sqrt{\frac{\gamma N^{1/3} R}{\chi^{1/6}}} \qquad (1)$$

Figure 2 shows clear agreement with this prediction.

To further verify our scaling prediction of the wavelength, the experiment was repeated for several different molecular weights (Fig. 3). The data is clearly consistent with our scaling prediction, which is shown as a solid curve. The only free parameter in the fit yields a value of $48\mu\text{m}^{0.5}$, which is close to the calculated value of ~ 3.1. This slight disagreement is likely related to the strong-segregation approximation used here (this can be loosely thought of as assuming a value for χ which is too large, if we lower χ our constant would clearly get larger).

The instability only occurs if the selected unstable wavelength can grow at a speed greater than that of the motion of the interface. This means that there is a critical range of speeds (or equivalently annealing times) where the fingering will occur. For the 36 kg/mol sample this occurs between 7 and 9 hours of annealing at 190°C. If we make the assumption that there is no reason for this critical velocity to depend on molecular weight (as the monomers and surface determine the dynamics) then the critical time depends only on the diffusion constant (i.e. $t_c = D/v_c$).

To learn more about the stability of the front we map out the location in time of the destabilizing transition as a function of N (see Fig. 4). In this plot we show regions of instability as an open circle with vertical error bars indicating the extent of the fingering region. All other regions indicate that only stable fronts were observed with AFM. The time to onset of instability appears to be a linearly increasing function of molecular weight, which reflects the decreasing mobility of longer chains compared to shorter ones. This is again what one would expect, as the diffusion constant of an unentangled polymer chain on a substrate scales linearly with N [17].

In conclusion, we have observed a novel instability of a spreading diblock copolymer monolayer. We show this fingering pattern to be a two dimensional analogy of the Mullins-Sekerka instability, and show a fair scaling agreement between these predictions and our measurements. Notably, we find that the finger spacing varies as the square root of the distance from the drop center to the fingering. The data is also consistent with a scaling of $N^1/6$. Finally we construct a stability diagram which locates the region of instability of several different molecular weights. This diagram indicates that the time at which fingering occurs scales linearly with molecular weight.

* Electronic address: dalnoki@mcmaster.ca

[1] M. Seul and D. Andelman, Science **267**, 476 (1995).
[2] A. Cazabat, F. Heslot, S. Troian, and P. Carles, Nature **346**, 824 (1990).
[3] J. Bechhoefer, P. Oswald, A. Libchaber, and C. Germain, Phys. Rev. Lett. **37**, 1691 (1988).
[4] A. P. Gast and Y. Monovoukas, Nature **351**, 553 (1991).
[5] T. Shinbrot, A. Alexander, and F. Muzzio, Nature **397**, 675 (1999).
[6] K. Shull, C. Flanigan, and A. Crosby, Phys. Rev. Lett. **84**, 3057 (2000).
[7] J. Nase, A. Lindner, and C. Creton, Phys. Rev. Lett. **101**, 074503 (2008).
[8] H. Xu, D. Shirvanyants, K. Beers, K. Matyjaszewski, A. V. Dobrynin, M. Rubinstein, and S. S. Sheiko, Phys. Rev. Lett. **94**, 237801 (2005).
[9] W. Losert, B. Q. Shi, and H. Z. Cummins, Proc. Natl. Acad. Sci. USA **95**, 431 (1998).
[10] P. de Gennes, Rev. Mod. Phys. **57**, 827 (1985).
[11] K. Migler, H. Hervet, and L. Leger, Phys. Rev. Lett. **70**, 287 (1993).
[12] W. W. Mullins and R. F. Sekerka, J. Appl. Phys. **35**, 444 (1964).
[13] J. S. Langer, Rev. Mod. Phys. **52**, 1 (1980).
[14] D. Ausserré, A. Picard, and L. Léger, Phys. Rev. Lett. **57**, 2671 (1986).
[15] L. Léger, M. Erman, D. A. A.M. Guiner-Picard, and C. Strazielle, Phys. Rev. Lett. **60**, 2390 (1988).
[16] H. Xu, D. Shirvanyants, K. Beers, K. Matyjaszewski, M. Rubinstein, and S. S. Sheiko, Phys. Rev. Lett. **93**, 206103 (2004).
[17] M. P. Valignat, G. Oshanin, S. Villette, A. M. Cazabat, and M. Moreau, Phys. Rev. Lett. **80**, 5377 (1998).
[18] A. N. Semenov, Sov. Phys. JETP **61**, 733 (1985).
[19] T. Ohta and K. Kawasaki, macromolecules **19**, 2621 (1986).

Eur. Phys. J. E **27**, 407–411 (2008)
DOI 10.1140/epje/i2008-10402-8

THE EUROPEAN PHYSICAL JOURNAL E

Kinetics of layer hopping in a diblock copolymer lamellar phase

A.B. Croll[1], M.W. Matsen[2], A.-C. Shi[1], and K. Dalnoki-Veress[1,a]

[1] Department of Physics & Astronomy and the Brockhouse Institute for Materials Research, McMaster University, Hamilton, ON, Canada
[2] Department of Mathematics, University of Reading, Whiteknights, Reading, UK

Received 3 November 2008
Published online: 9 December 2008 –

Abstract. In the ordered state, symmetric diblock copolymers self-assemble into an anisotropic lamellar morphology. The equilibrium thickness of the lamellae is the result of a delicate balance between enthalpic and entropic energies, which can be tuned by controlling the temperature. Here we devise a simple yet powerful method of detecting tiny changes in the lamellar thickness using optical microscopy. From such measurements we characterize the enthalpic interaction as well as the kinetics of molecules as they hop from one layer to the next in order to adjust the lamellar thickness in response to a temperature jump. The resolution of the measurements facilitate a direct comparison to predictions from self-consistent field theory.

PACS. 83.80.Uv Block copolymers – 68.47.Mn Polymer surfaces – 82.35.Jk Copolymers, phase transitions, structure – 68.55.J- Morphology of films

Often the most fascinating features of nature are rooted in the complexity and order found in self-assembling patterns. The innate interest in self-assembly, coupled with the technological need for simple cost-effective templates results in a significant research effort to understand pattern formation [1]. Of the many self-assembling nanoscale polymeric structures, some of the most remarkable are formed by block copolymers [2,3]. Block copolymers are long chain molecules made up of segments of different chemical constituents joined together by a covalent bond. In the simplest case, a block of fN segments is attached to another block of $(1-f)N$ segments to form a diblock copolymer. Because of the general incompatibility of the chemically distinct blocks, the molecules exhibit amphiphilic properties: that is, the blocks tend to segregate into structures that minimize contact between unlike segments. These molecules will typically self-assemble into long-range periodically ordered morphologies composed of nanosized domains, when cooled below an order-disorder transition (ODT). The composition of the molecule, f, sets the preferred curvature of the internal interfaces which, in turn, controls the geometry of the resulting morphology; symmetric diblocks ($f \sim 1/2$) prefer zero curvature resulting in a simple lamellar phase, where the incompatible domains form flat alternating layers. The repeat period, L, is on the order of the relaxed molecular size (*i.e.*, the polymer radius of gyration, $R_g \sim 10\,\mathrm{nm}$), but the precise value of L is controlled by the product, χN, where the Flory-Huggins parameter, χ, is a temperature-dependent quantity that specifies the incompatibility of the unlike segments.

Here we examine thin films of a symmetric diblock copolymer, which form a stack of lamellae oriented parallel to the substrate. Using a simple optical measurement, we are able to monitor changes in the domain size, L, *in situ* with an unprecedented sensitivity. By comparing the measured L with predictions from self-consistent field theory (SCFT), we extract the temperature dependence of χ and verify the technique. With the methodology established, we measure the equilibration of L as the lamellae respond to a sudden temperature jump. The resolution of the experiments facilitates a direct comparison of the data with SCFT, which provides a quantitative, parameter-free measure of the kinetic energy barrier, $\Delta\epsilon$, for an individual molecule to hop between adjacent layers.

The kinetics of molecular motion in structured morphologies is of wide interest [4–7]. It is relevant to virtually all complex liquids and biological systems; such as the exchange of molecules between layers in smetic liquid crystals and between the inner and outer layers of lipid membranes. In the model system of block copolymer melts, Lodge and co-workers have tried to differentiate between lateral diffusion where the molecules move with their junction point on the same interface, and perpendicular diffusion where the junction point jumps between neighboring interfaces [8]. In our experiment, the rate of change in the

[a] e-mail: dalnoki@mcmaster.ca

domain spacing of our defect-free thin films is controlled solely by the rate at which the molecules hop between layers, since lateral diffusion does not contribute to changes in L. A decrease in L, for example, requires molecules to move upward through the layers eventually adding to the topmost incomplete layer —a reservoir, which adjusts its area accordingly.

The main difficulty in quantitatively relating theory to experiment is obtaining the temperature dependence of χ. This dependence is often determined by measuring the ODT of symmetric diblock copolymers of different N, and matching to Leibler's mean-field prediction, $(\chi N)_{\mathrm{ODT}} = 10.495$, with $\chi = A/T + B$ expressed in terms of the fitting parameters, A and B. However, it is known that fluctuations play an important role in the location of the ODT, and additional theory is used to supplement the prediction of $(\chi N)_{\mathrm{ODT}}$ [9,10]. Another common approach is to perform the comparison on symmetric binary blends, but unfortunately this does not always produce a consistent result [11]. Regardless of the methodology, the comparison should be performed on some quantity for which both the experiment and theory are accurate. Our use of the domain size L is particularly ideal [12], because not only can we measure it accurately, it is also considered to be one of the most reliable predictions of SCFT.

The molecule used in our experiment is a monodisperse (polydispersity index of 1.09), symmetric ($f = 0.50$), diblock copolymer polystyrene-poly(2-vinyl pyradine), with a molecular weight of $M = 16.5\,\mathrm{kg/mol}$ (Polymer Source). Thin films of various thicknesses were prepared by spin-coating the polymer from toluene or chloroform solution onto silicon substrates with the native oxide layer present, which were cleaned by super-critical CO_2 (Applied Surface Technologies) and UV-ozone. Upon annealing the sample below the ODT temperature, a surface topography results due to the lamellar confinement —the molecules must exist within lamellae of a preferred thickness, L. If an integer number of n lamellae happens to be commensurate with the film thickness (*i.e.*, $h = nL$), then the film adopts a flat featureless surface. When there is a small amount of extra material, the film creates a topography of isolated islands of height L on top of the n complete layers. Further material causes the islands to grow eventually merging into an interconnected bicontinuous structure. As the low areas are gradually filled in, the topography is best described as a film of thickness $h = (n+1)L$ with isolated holes of depth L. Ultimately, the holes fill in producing again a flat uniform film, but now with $(n+1)$ complete layers [13]. These surface topographies: islands, bicontinuous networks and holes, are readily observed with simple optical microscopy.

Even with a fixed amount of material, the topography of the film surface varies with temperature because of the effect that the temperature dependence of χ has on the preferred lamellar thickness, L. The equilibrium thickness results from a delicate balance between the energy penalty of the internal interfaces separating the unlike domains (favoring large L) and the entropic cost of stretching the blocks so as to fill the center of each domain (favoring small L). A decrease in temperature, for example, causes an increase in χ, which in turn amplifies the interfacial tension resulting in thicker domains. Because the polymer melt can be treated as incompressible, the increase in L among the complete layers must be accommodated by removing molecules from the topmost layer, thus reducing its area (see Fig. 1(a)). The change in area can be calculated by writing the volume of film within some large field of view as $V = L(T)[nA_f + a(T)]$, where n is the number of complete layers each of area A_f and $a(T)$ is the total area of the upper incomplete layer within the field of view. Since the thermal expansion is a small contribution [14], V can be treated as constant, and the lamellar thickness can be written with respect to a reference temperature, T_0, as

$$\frac{L(T)}{L(T_0)} = \frac{nA_f + a(T_0)}{nA_f + a(T)}\,. \tag{1}$$

Using the observed area in this way, we can accurately infer tiny variations in L, because the topography of the topmost surface results from the change in thickness of *all* the lamellae in the film [15].

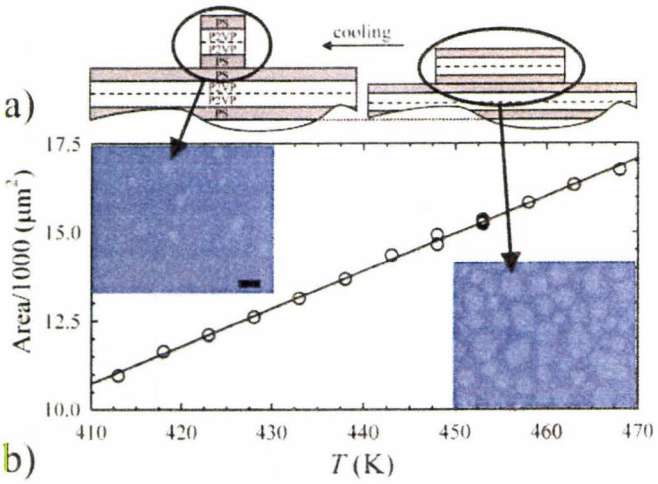

Fig. 1. a) Schematic cross-section of a film illustrating the decrease in island area and increase in lamellar thickness upon cooling the film. b) Total area of surface structures as a function of temperature for a film with $n = 2$ layers. Optical images in the inset collected at 433 K and 463 K for a film with $n = 7$ layers (20 μm scale bar).

In our experiment, samples are placed on a hot stage in a nitrogen atmosphere and an optical microscope is used to observe any changes in the area of the topmost layer as the temperature is slowly changed. After each change in temperature, the sample is allowed to equilibrate for as long as is necessary for the surface topography to stop changing. Figure 1(b) shows the change in area of the topmost layer as the temperature is decreased from 468 K to 413 K. Over this range in temperature the area of the islands is seen to vary linearly with a slope of $106\,\mu\mathrm{m}^2/\mathrm{K}$. Analogous measurements were conducted for film thicknesses ranging up to $n = 7$ and with surface topographies ranging from islands to holes. Figure 2 shows the data from all these films scaled according to equation (1); there

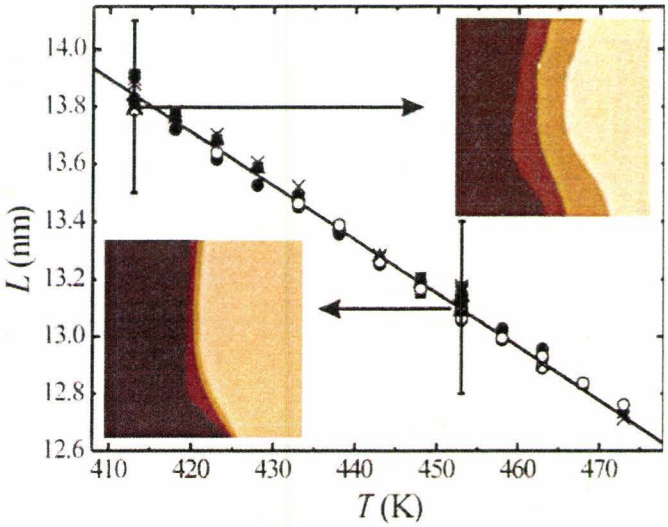

Fig. 2. Master plot of many block copolymer films ranging in thickness from $n = 2$ to 7 lamellae (2-squares, 3-stars, 4-circles, 6-triangles, 7-crosses). The curve is a fit to the function discussed in the text. The inset shows two AFM images of the same film at different temperatures with the AFM error shown by the error bars (scan size $10 \times 10\,\mu$m).

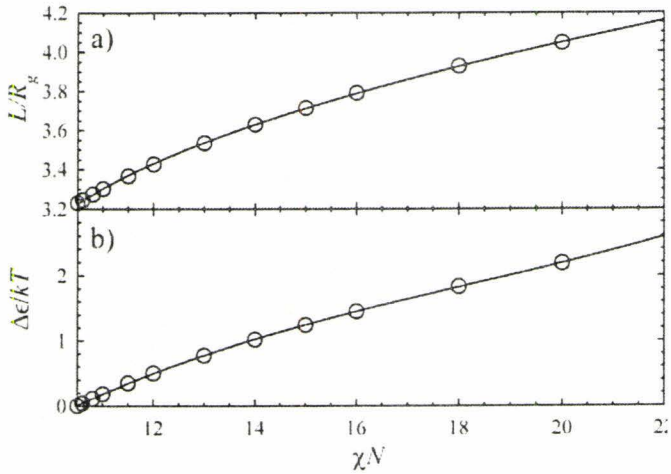

Fig. 3. Self-consistent field theory calculations of a) the lamellar spacing and b) the energy barrier associated with a molecule hopping from one layer to the next.

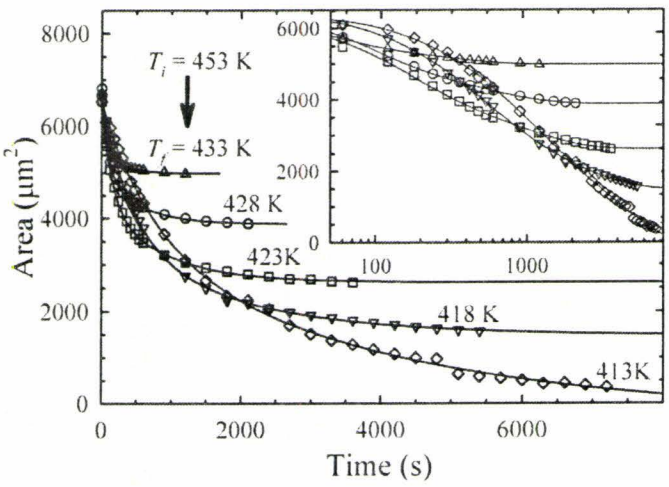

Fig. 4. Experiments following the change in the area of the top layer as the temperature is quenched from $T_i = 180\,^\circ$C to T_f as indicated, for a film with $n = 7$ complete layers. The lines represent fits to the exponential decay, equation (4).

is a near perfect collapse of the data onto a single master curve. This implies that the substrate interface has a negligible effect on L —more precisely, we can infer that the thickness of each and every layer is indicative of the bulk lamellar spacing despite its proximity to the substrate. We note that this result is in complete agreement with SCFT predictions [16].

Although the optical measurements of the area are very sensitive to the ratio L/L_0, they do not provide an absolute value for L. AFM is used here to set the absolute scale for L_0, we use $L(453\,\mathrm{K}) = 13.1\,\mathrm{nm}$ as this reference. This absolute reference is obtained from AFM measurements of a number of lamellae. The very small change in thickness of lamella makes the AFM measurement extremely error prone, as indicated by the relatively large error bars in Figure 2. Another disadvantage of the AFM measurement is that lamellae that are parallel to a substrate can only be measured at a lamellar edge. An edge is where one would expect to see the most deviation from the "bulk" lamellar thickness. This highlights the advantages of the optical measurement —it is simple and very accurate, as one can average the change over many surface domains of different sizes and furthermore the n-layers amplify the effect on the topmost feature.

Numerical solutions of the self-consistent field theory show that L/R_g is an increasing function of χN, which is extremely well fit by

$$L/R_g = 2.8 + \sqrt{0.15(\chi N - 9.2)}, \qquad (2)$$

shown in Figure 3(a) by the solid curve. Note that the conventional power law fit, $L/R_g \sim (\chi N)^m$, is a relatively inaccurate approximation, which may explain the wide range of exponents, m, quoted in the literature. Fitting equation (2) to the experimental results in Figure 2 with $R_g = 3.44\,\mathrm{nm}$ (since both blocks are structurally similar, R_g is obtained from polystyrene parameters [17]), we obtain

$$\chi = \frac{(97 \pm 2)\,\mathrm{K}}{T} + (-0.11 \pm 0.01), \qquad (3)$$

in close agreement with previous measurements [10,18].

Further insight into the process by which lamellae form and adjust their length scale with temperature is available through experiments which probe the dynamics of the transition from equilibrium at T_i, and a quench to T_f. Molecules from one lamella can penetrate into another lamella by overcoming an energy barrier $\Delta\epsilon$ —roughly, the energy associated with a block entering a matrix of the unfavorable block [19]. Figure 4 shows the response of the area of the topmost layer $(n + 1)$ as the temperature is dropped from $T_i = 453\,\mathrm{K}$ to T_f for a film with $n = 7$. With the drop in temperature, the lamella becomes more

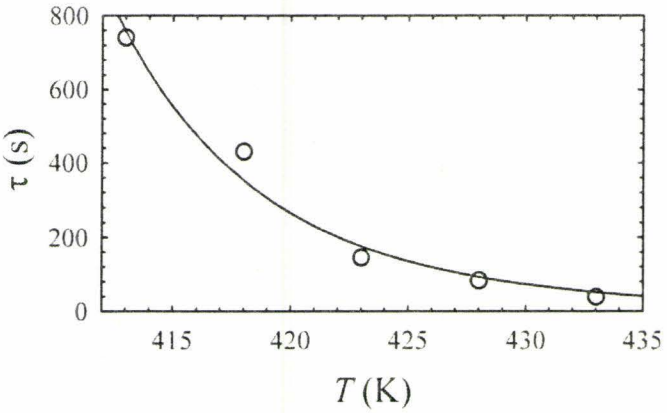

Fig. 5. Time constant associated with the probability of molecules hopping from one layer to the next, τ, as a function of temperature, T. The line is a fit to equation (5).

strongly segregated, and L increases resulting in a pressure difference that is equilibrated by molecules hopping from one lamella into another. This results in a decrease in $a(t)$ with time as molecules from the topmost layer, which acts as a reservoir, empty into the n layers below.

A model can be constructed to describe the decay of the area of the islands, $a(t)$, from a_i to a_f resulting from the temperature quench. For modest temperature jumps, it is natural to assume that the rate of change is $a'(t) \propto [a(t) - a_f]$, which leads to exponential decay,

$$a = (a_i - a_f)\exp(-t/\tau) + a_f\,. \tag{4}$$

In Figure 4, we fit the data to equation (4) plus an additional long-time exponential relaxation. The additional relaxation is attributed to the gradual Ostwald ripening of the islands or holes, and occurs on a time scale that is independent of and much larger than that of the hopping mechanism.

The symbols in Figure 5 denote the time constants, τ, extracted from our fits at the various temperatures, T. The changes in τ are dictated by two important temperature-dependent contributions. The first contribution, the frequency with which molecules *attempt* to pass between layers, is represented by the temperature dependence of molecular motion, and is given by the Vogel-Fulcher expression, $\exp[-T_A/(T-T_V)]$. Because the chemical structures of polystyrene and poly(2-vinyl pyridine) are so similar [20], we use the values, $T_A = 1250$ and $T_V = 320$, of polystyrene homopolymer [17]. The second contribution, the success rate with which the molecules diffuse across lamellae, is a thermally activated process $\tau \propto \exp(\Delta\epsilon/kT)$, where $\Delta\epsilon$ is the energy barrier associated with molecules hopping between layers. Thus the time constant can be expressed as

$$\tau = \tau_0 \exp[T_A/(T - T_V)]\exp(\Delta\epsilon/kT), \tag{5}$$

where τ_0 is a temperature-independent quantity that depends on details such as the total number of layers, n. Returning to the SCFT, we calculate $\Delta\epsilon$ by examining the free energy of a single polymer in the self-consistent fields as its junction point is dragged from one interface to another. Note that the SCFT automatically accounts for changes in the block copolymer conformations as the molecule passes between layers. The theoretical result, plotted in Figure 3(b) as a function of χN, is then converted to a function of T using our fit of χ in equation (3) with $N = 158$. The solid curve in Figure 5 shows the theoretical expression in equation (5) fit to the data using only one free parameter ($\tau_0 = (1.3 \pm 0.1) \times 10^{-4}$ s). The excellent agreement between the theory and experiment provides a useful consistency check between the information gained from the static and kinetic experiments.

In conclusion, we have used a simple optical technique to measure the area of the surface structure of symmetric diblock copolymer lamellae. As the temperature is varied, the balance between the entropic stretching of chains and the enthalpic repulsion between the two chemically distinct polymer blocks results in a change in the thickness of the lamellae. When the lamellar thickness changes, material from the topmost layer acts as a *reservoir* changing its area accordingly. This reservoir responds to all the layers thus amplifying any change in the lamellar thickness. Because of this amplification, the simple area measurement of the top layer can extract changes in the lamellar thickness with unprecedented resolution. Our study begins by comparing the equilibrium thickness of lamellae as a function of temperature to predictions from self-consistent field theory; from this, we obtain the temperature dependence of the Flory-Huggins χ parameter (see Eq. (3)). In the second part of our study, we switch from equilibrium measurements to dynamics; by measuring the rate with which the area of the topmost layer changes in response to a temperature jump, we obtain a time constant associated with molecules passing over the energetic barrier as they hop from one layer to the next. The relaxation data is fit with a simple model, which verifies both the model and the consistency between the results obtained for both the equilibrium and dynamic measurements. For both sets of experiments, a simple optical microscopy observation is used to obtain parameters describing the motion of the diblock chains on a molecular level.

The authors thank Prof. Edward Kramer for valuable discussions. Financial support from NSERC and the ACS PRF are gratefully acknowledged.

References

1. M. Seul, D. Andelman, Science **267**, 476 (1995).
2. F.S. Bates, G.H. Fredrickson, Annu. Rev. Phys. Chem. **41**, 525 (1990).
3. G.H. Fredrickson, F.S. Bates, Annu. Rev. Mater. Sci. **26**, 501 (1996).
4. Y. Kang, J. Walish, T. Gorishnyy, E. Thomas, Nature Mater. **6**, 956 (2007).
5. D. Constantin, P. Oswald, Phys. Rev. Lett. **85**, 4297 (2000).
6. H.C. Gaede, K. Gawrisch, Biophys. J. **85**, 1734 (2003).

7. R. Blinc, M. Burgar, M. Luzar, J. Pirš, I. Zupančič, S. Žumer, Phys. Rev. Lett. **33**, 1192 (1974).
8. T.P. Lodge, M.C. Dalvi, Phys. Rev. Lett. **75**, 657 (1995).
9. G.H. Fredrickson, E. Helfand, J. Chem. Phys. **87**, 697 (1987).
10. M. Schulz, A. Khandpur, F.S. Bates, K. Almdal, K. Mortensen, D.A. Hajduk, S.M. Gruner, Macromolecules **29**, 2857 (1996).
11. W.M. Maurer, F.S. Bates, T.P. Lodge, K. Almdal, K. Mortensen, G.H. Fredrickson, J. Chem. Phys. **109**, 2989 (1998).
12. A.S. Zalusky, R. Olayo-Valles, J.H. Wolf, M.A. Hillmyer, J. Am. Chem. Soc. **124**, 12761 (2002).
13. P. Green, R. Limary, Adv. Colloid Interface Sci. **94**, 53 (2001).
14. Thermal expansion opposes and contributes less than 10% of the measure effect, *i.e.* lamellae decrease in thickness with increasing temperature.
15. H. Bodiguel, C. Fretigny, Eur. Phys. J. E. **19**, 185 (2006).
16. M.W. Matsen, J. Chem. Phys. **106**, 7781 (1997).
17. J.E. Mark (Editor), *Physical Properties of Polymers Handbook* (American Institute of Physics, 1996).
18. K.H. Dai, E.J. Kramer, Polymer **35**, 157 (1994).
19. H. Yokoyama, Mat. Sci. Eng. R. **53**, 199 (2006).
20. C.E. Eastman, T.P. Lodge, Macromolecules **27**, 5591 (1994).

Ordering of a lamella forming fluid near an interface

Andrew B. Croll, An-Chang Shi, and Kari Dalnoki-Veress*
Department of Physics & Astronomy and the Brockhouse Institute for Materials Research, McMaster University, Hamilton, ON, Canada
(Dated: December 7, 2008)

By using wedged thin films, we have measured the effect of interfaces on the ordering of an anisotropic fluid in real space. Symmetric diblock copolymers can form an ordered lamellar fluid, and the preference of the substrate for one of the blocks can induce order well into the disordered bulk phase. The induced order decays away from the substrate with a lengthscale that diverges at the bulk ordering transition. Ordering and disordering kinetics is found to differ: all layers relax identically upon disordering; whereas, the formation of lamellae is found to vary with the distance from the substrate, and can be understood from the time-dependent Ginzberg-Landau theory.

PACS numbers: 83.80.Uv, 68.47.Mn, 82.35.Jk, 68.55.J-

Interest in polymers at interfaces is rooted in the varied effects that have been observed, some of which are not yet fully understood. Bulk morphologies are often modified near interfaces due to finite size or confinement effects, providing an alternate route to patterning. A striking example is that of binary mixtures, where phase separation has been found to occur preferentially near an interface – *surface directed spinodal decomposition* [1]. Similarly, diblock copolymers, long chain molecules made up of segments of different chemical constituents joined together by a covalent bond, can order in the presence of an interface [2–5]. Just as a blend of two fluids can phase separate, block copolymers will also phase separate when cooled below the order-disorder transition (ODT) [7]. However, the connectivity of the two blocks restricts the separation to a molecular lengthscale. The details of the geometry of the resulting domains is set by the number of monomers, N, the ratio of the lengths of the two blocks, f, and the Flory-Huggins interaction parameter, χ, which specifies the incompatibility of the unlike segments and varies inversely with temperature. In the case of a symmetric diblock copolymer, $f = 1/2$, and the resulting morphology is that of alternating lamellae of a-rich and b-rich domains. In the bulk, lamella will self-assemble out of the isotropic melt when $\chi N > (\chi N)_{ODT}$.

When the block copolymer melt is near a wall that has some affinity for one of the two monomers this simple description breaks down [3–6]. If the a monomers prefer the substrate, then even for temperatures, $T > T_{ODT}$, corresponding to $\chi N < (\chi N)_{ODT}$, local order is induced. An a-rich region forms near the interface, and due to the connectivity of the molecules, this forces a b-rich region to form. In analogy with surface directed spinodal decomposition [1], beyond the b-rich domain there is not an abrupt transition to a purely disordered melt, but a slow screening of the surface over progressively less highly concentrated a-rich and b-rich domains. Near the ODT the system is only weakly segregated (i.e. the interface between the a and b domains is not sharp) and we can write a decaying oscillatory concentration gradient as a function of the distance from the interface as [3–5]

$$\psi(z) \sim \exp(-z/\xi)\cos(\Omega z + \phi); \tag{1}$$

where Ω sets the period of the concentration profile and scales with the radius-of-gyration, R_g, of the molecule, ϕ depends on the strength of the block-interface interaction, and the the concentration decays into the bulk with a characteristic length given by

$$\xi = \frac{2R_g}{\sqrt{\chi N - (\chi N)_{ODT}}}. \tag{2}$$

This form was first predicted by Fredrickson [4], verified with the self-consistent field theory of Shull [5], and observed with scattering [2, 3].

Measurements of the concentration profile are generally inferred through fits to neutron or x-ray scattering profiles [2, 3]. These types of experiments are invaluable in studying the internal structure of a material, although the inherent complexity and ambiguity associated with modeling the scattering make complementary methods of great value. Here we present a simple alternative: we observe perturbations in the surface of a wedged diblock film caused by its internal concentration profile. Not only does this enable an accurate determination of ODT using only an optical microscope, but we have for the first time measured the extent of the ordering induced by the substrate on an isotropic diblock melt in real-space. Furthermore, we present measurements on the kinetics of ordering which which reveal that the ordering and disordering kinetics differ, and are well described by theory.

The polymer used in this study is a monodisperse (polydispersity index of 1.09), symmetric ($f = 0.50$), polystyrene-poly(2-vinyl pyradine) diblock copolymer, with a molecular weight of $M = 16.5$ kg/mol, which corresponds to $N = 158$ (Polymer Source). Samples with a gradient in the film thickness were prepared by allowing a capillary wedge to form between a silicon substrate with the native oxide layer present, and a horizontal glass capillary (using a dilute polymer solution). Samples were

*Electronic address: dalnoki@mcmaster.ca

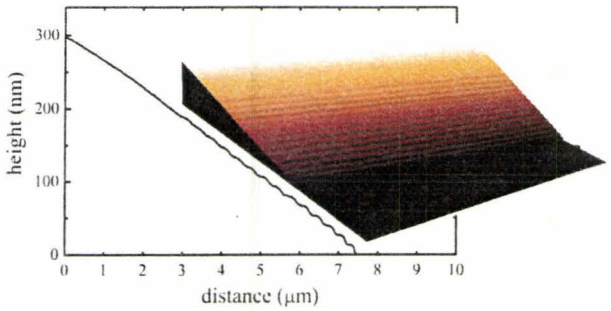

FIG. 1: Atomic force microscopy topography image (10 μm $\times$10 μm) and a height trace of a sample rapidly quenched to room temperature after equilibration at 438 K.

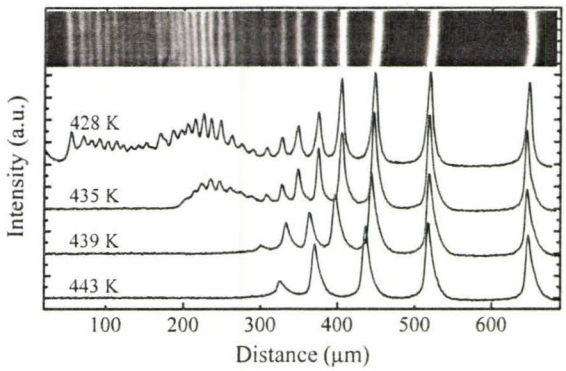

FIG. 2: A dark-field image of a wedged film at 428 K is shown in the inset. Typical intensity profiles through such images, taken at the temperatures indicated, are shown (shifted vertically for clarity).

heated using a microscope hot stage (Linkam Scientific) and observed with optical microscopy (Olympus BX51) and atomic force microscopy (AFM) (Veeco Caliber).

The films form discrete lamellar steps when ordering in order to accommodate the wedge geometry, see Fig. 1. Standard dark-field microscopy is ideal for observing the steps: light is incident on a sample at a large angle from the film normal and observations are made along the normal. As T is decreased towards T_{ODT}, ordered lamella form and the surface of the wedged films is broken by the layer edges of the anisotropic liquid. The lamellar steps are small ($\sim$ 13.5 nm [8]) and form ideal scattering sites as is shown in the inset of Fig. 2. Upon cooling we observe the lamellar edges in the intensity traces of Fig. 2, which form first near the substrate (i.e. only 5 ordered layers are observed at 443 K), and then order sets in further into the bulk of the film as T decreases and hence ξ increases. In Fig. 2 the film is thickest on the left, i.e. order sets in on the right. We note that the magnitude of the intensity peaks does not solely reflect the degree of order, but also a convolution of thin film interference effects. The scattering provided by edges and the resulting intensity profile allows for a very simple method to track the height above the substrate $L(T)$ of the highest observable ordered layer in a sample. As the temperature is changed the sample is allowed to equilibrate, the intensity profile obtained, and the number of peaks in this curve corresponds to the number of ordered layers in the sample. This methodology not only allows us to map out the equilibrium structure near ODT, but to follow the dynamics of ordering in real-time.

Before we analyse the ordering in detail, several qualitative observations must be made. 1) When $T > T_{ODT}$ the sample is partially ordered near the substrate and we never observe scattering at the thickest part of a wedged sample. This lack of lamellar steps is also verified with AFM measurement, which allows us to conclude that ordering is dominated by the substrate rather than air interface. This is consistent with the fact that the two blocks have very similar affinity for the air interface as the surface tensions are very similar. 2) T_{ODT} is determined to be 433 K from observation of the temperature at which a sample becomes ordered at its thickest point. 3) Measurements of the appearance or disappearance of each layer with a change in T can be made, and reveal a significant difference in kinetics between disordering and ordering, with ordering being the slower process. 4) An edge appearing in the transition region from order to disorder along the gradient of the film has a lower intensity than when that same edge is fully ordered at a lower T. The latter observation suggests a relationship between the scattering intensity and the degree of order present in a sample given by the concentration envelope, $\sim \exp(-z/\xi)$, of Eq. 1. The lamellae scatter light because the edges are well defined steps, smoothed by surface tension. The intensity of light scattered from an edge correlates with the degree of ordering in a layer. This can be verified with AFM as shown in Fig. 1 for a sample equilibrated at 438 K, just above T_{ODT}. The lamellar edges become progressively less well defined as one moves away from the substrate and the concentration amplitude decreases. No ordering is observable with AFM beyond 14 layers, which corresponds exactly with the last *optically* observable layer at 438 K.

In order to analyze this data we make the following assumption: a layer edge geometry is related to the amplitude of $\psi(z)$. More precisely, the number of observable ordered layers corresponds to a depth of order into the bulk, L, which we assume to be proportional to the decay length, ξ. The number of observable ordered layers as a function of temperature is then a measure of the concentration profile. In Fig. 3 we plot the dimensionless lengthscale L/R_g, where $R_g = 3.44$ nm is the radius of gyration of the molecules (we have accounted for the change in lamellar spacing with T, which is $\sim$ 5% over the entire range) [8]. The inset to Fig. 3 shows the data plotted as suggested by Eq. 2. Contrary to the prediction that the data should fall on a single straight line, there are two distinct linear regions, each with a different slope. This bimodal scaling is consistent with a 'curvature' pre-

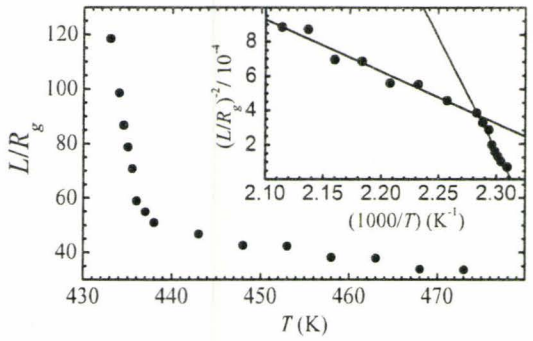

FIG. 3: Height of the topmost observable ordered lamella normalised to R_g as a function of temperature for a typical sample. The inset shows the scaling of $L(T)$ as suggested by Frederickson [4] which reveals two linear regimes.

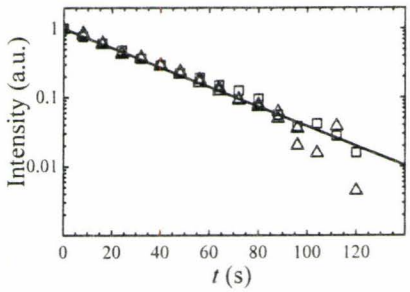

FIG. 4: The normalised intensity of light scattered from a lamellar edge as a function of time while disordering. The intensity decays as the sample is quenched from well ordered at 428 K to disordered at 435 K. Three lamellae are shown corresponding to the 19-21st lamella away from the substrate.

viously observed by Menelle and coworkers [3]. To understand each region we must recognize that the two surfaces (substrate and air) compete to set the scale of the order in a sample. At low temperatures the stronger ordering of the substrate is dominant throughout the sample, and the highest visible layer is directly proportional to the decay length, $L = k\xi$. We can ignore the air interface because the surface tension of the two components is nearly identical i.e. the value of the concentration at the air boundary, $\psi \sim \cos(\phi_{air})$ is small relative to the substrate effect. We can directly verify this assumption: Eq. 2 and the Flory-Huggins parameter, which is typically written as $\chi = A/T + B$, results in $L^{-2} \sim A/T - A/T_{ODT}$. From the ratio of the slope to the intercept we obtain $T_{ODT} = 433 \pm 0.4$ K, consistent with the divergence of $L(T)$ in Fig. 3. When the temperature becomes higher the substrate effect damps out more rapidly, and ξ decreases. Eventually, the assumption made above, that the substrate amplitude dominates even at the air interface is invalid (i.e. $\exp(-h/\xi) < \cos(\phi_{air})$; with film thickness h). Thus, the ordering at the air surface suppresses the highest observable layer since ordering at the air interface does not form step edges which can be observed in the experiment. In this case the observed number of layers $L = (k - k')\xi$, and the slope in the high temperature region of the inset in Fig. 3 is reduced. This transition from the substrate dominated regime to that where the air interface contributes is clearly seen in the crossover in the inset of Fig. 3.

The original mean field predictions of Leibler set the value of $(\chi N)_{ODT} = 10.495$ [9]; however, imposing the value of the spinodal point from a mean field theory that does not account for fluctuations is not reasonable [10]. We have previously measured $\chi = 97/T - 0.11$ for the identical system [8]. We consider the combination of these measurements to be an accurate, and stress free, determination of $(\chi N)_{ODT}$. For the system studied, $N = 158$, and we find that $\chi N_{ODT} = 18.0 \pm 1$. This value is reasonable since fluctuation effects drive the transition higher than Leibler's $(\chi N)_{ODT}$, though this quantity is not yet quantitatively predictable [10, 11]. For example, the work of Fredrickson and Helfand suggests that $(\chi N)_{ODT}$ is increased from the mean field value of 10.495 to a value given by $(\chi N)_{ODT} = 10.495 - 41.022(Na^6v^{-2})^{-1/3}$; where the monomeric parameters a and v are the segment length and the segmental volume. A reasonable estimate of $a^3/v \sim 1$, gives $(\chi N)_{ODT} \sim 18$, which is in agreement with the measured value.

The methodology presented here provides an excellent window into ordering dynamics. The change in the intensity, I, of the scattered light from the edge of a lamellae is proportional to the change in segregation of the a and b domains, $\Delta I(T) \sim \Delta[\exp(-z/\xi(T))]$. Thus, by observing the intensity of a given lamellar edge in time we gain information about the dynamics of each layer. In Fig. 4, we plot the normalised intensity, $\Delta I(t)/\Delta I$, for several lamellae as a function of time, after a quench from a well-equilibrated ordered state at 428 K to 435 K, a temperature above the ODT. One can easily identify the exponential nature of the dynamics with a time constant of $\tau = 32.8 \pm 0.4$ s. In short, as the system is quenched into the isotropic state, all the ordered lamellae disorder at the same rate and independent of the distance from the substrate, as expected since the relaxation is viscosity dominated.

In Fig. 5, we plot the intensity normalised to that of the fully ordered state for the five lamellae ranging from the 18th to the 22nd from the substrate. A disordered sample at 435 K is quenched to the ordered state at 433 K. Here we observe a significant difference from the disordering process: the intensity rises asymptotically and the process of ordering takes longer for lamellae that are further from the substrate. The ordering kinetics can be understood from the time-dependent Ginzberg-Landau theory as extended to diblocks by Ohta and coworkers [12]. For a lamellar structure, the amplitude of the concentration profile, $A(t)$, evolves towards the ordered equilibrium amplitude, A_O, according to the kinetic equation, $dA/dt \sim (A_O^2 - A^2)A$. Defining $y(t) = A(t)/A_O$, the solution to this equation provides the evolution from the initial amplitude, y_0, as $y = 1/\sqrt{1 + \exp[-2(t - t_0)]}$; with $t_0 = \ln(1/y_0^2 - 1)/2$. We emphasize that the solutions for

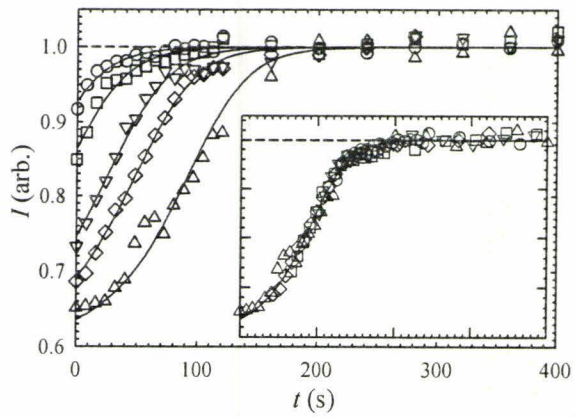

FIG. 5: The light intensity scattered from a lamellar edge as a function of time while ordering. The five lamellae are the 18th-22nd from the substrate after a quench from 435 K to 433 K. The solid lines correspond to the best fit of Eq. 3, with $I_D = 0.6$, $\omega = 45$ s, and t_0 given in Fig. 6. The inset shows the master-curve, after applying the shift factors, t_0.

different initial concentrations are simply shifted by the time offset t_0. Assuming that $I \sim A$,

$$I = I_D + \frac{I_O - I_D}{\sqrt{1 + \exp[-2(t - t_0)/\omega]}}; \qquad (3)$$

where I_D and I_O are the intensities measured for the fully disordered and ordered state, and ω is the time constant which represents the width of the transition (note that $I_D \neq 0$ if there is a nonzero background intensity as in this experiment). The fit of Eq. 3 to the data is excellent as shown in Fig. 5, and the shift factors thus obtained can be applied to provide the master-curve shown in the inset (values of t_0 shown in Fig. 6). The initial intensities follow the concentration amplitude, which is given as a function of the distance from the substrate by Eq. 1 as $y_0 = a\exp(-z/\xi)$; with $a < 1$. To first order, the plot of the shift factor, t_0, as a function of the distance from the substrate is linear with a slope given by $\omega/a^2\xi$. Indeed Fig. 6 is linear and the best fit line has a slope of 30 ± 2 s. With this slope, the best fit value $\omega = 45$ s and taking $a \sim 0.5$, one obtains a decay length of ~ 10 which is entirely reasonable given that at 435 K, the last observable lamellae is ~ 20.

In conclusion, we have presented a simple approach for the study of the effect of interfaces on the ordering of a lamella forming fluid. The degree of order is probed with dark field optical microscopy by light scattering from the lamellar edges at the surface of wedged diblock copolymer films. Even in the disordered state, the sample can have order induced by the presence of an interface which decays away from the perturbation. We have, for the first time, measured this decay in real space and the dynamics of the ordering/disordering process. With a symmetric diblock copolymer, we provide several methods of

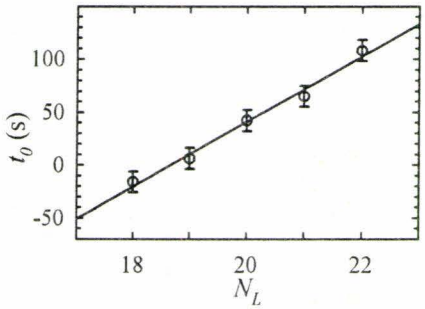

FIG. 6: Shift factors t_0 for lamellae 18 to 22 (see Fig. 5).

locating T_{ODT}, and determine that $(\chi N)_{ODT} = 18.0 \pm 1$. The different measures of T_{ODT} show excellent agreement with each other, and the concentration profile is in agreement with the scaling predicted by Fredrickson [4]. It is found that the disordering kinetics is limited by viscous processes and not influenced by the substrate. Experiments probing ordering are in full agreement with the kinetics predicted by the time-dependent Ginzberg-Landau theory of Ohta and coworkers [12].

The authors thank Prof. Mark Matsen for valuable discussions. Financial support from NSERC and the ACS PRF are gratefully acknowledged.

[1] R. A. L. Jones, L. J. Norton, E. J. Kramer, F. S. Bates, and P. Wiltzius, Phys. Rev. Lett., **66**, 1326 (1991).
[2] M. D. Foster, M. Sikka, N. Singh, F. S. Bates, S. K. Satija, and C. F. Majkrzak, J. Chem. Phys., **96**, 8605 (1992).
[3] A. Menelle, T. P. Russell, S. H. Anastasiadas, S. K. Satija, and C. F. Majkrzak, Phys. Rev. lett., **68**, 67 (1992).
[4] G. H. Fredrickson, Macromolecules, **20**, 2535 (1987).
[5] K. R. Shull, Macromolecules, **25**, 2122 (1992).
[6] H. Tan, D. Yan, and A.-C. Shi, Macromolecules, **37**, 9646 (2005).
[7] G. H. Fredrickson, and F. S. Bates, Annu. Rev. Mater. Sci., **26**, 501 (1996).
[8] A. B. Croll, M. W. Matsen, A.-C. Shi, and K. Dalnoki-Veress, Euro. Phys. J. E, in press.
[9] L. Leibler, Macromolecules, **13**, 1602 (1980).
[10] G. H. Fredrickson and E. Helfand, J. Chem. Phys., **87**, 697 (1987).
[11] O. Vassiliev and M. W. Matsen, J. Chem. Phys., **118**, 7700 (2003).
[12] K. Yamada, M. Nonomura, T. Ohta, Macromolecules, **37**, 5762 (2004).